NIST Technical Note 1462

A Four-Terminal Current Shunt with Calculable AC Response

O. B. Laug
T. M. Souders
B. C. Waltrip

NIST National Institute of Standards and Technology • Technology Administration • U.S. Department of Commerce

NIST Technical Note 1462

A Four-Terminal Current Shunt with Calculable AC Response

O. B. Laug
T. M. Souders
B. C. Waltrip
Electronics and Electrical Engineering Laboratory
National Institute of Standards and Technology
Gaithersburg, MD 20899-8111

August 2004

U.S. Department of Commerce
Donald L. Evans, Secretary

Technology Administration
Phillip J. Bond, Under Secretary for Technology

National Institute of Standards and Technology
Arden L. Bement, Jr., Director

National Institute of Standards and Technology Technical Note 1462
Natl. Inst. Stand. Technol. Tech. Note 1462, 48 pages (August 2004)
CODEN: NSPUE2

U.S. GOVERNMENT PRINTING OFFICE
WASHINGTON: 2002

For sale by the Superintendent of Documents, U.S. Government Printing Office
Internet: bookstore.gpo.gov — Phone: (202) 512-1800 — Fax: (202) 512-2250
Mail: Stop SSOP, Washington, DC 20402-0001

Table of Contents

List of Figures

List of Tables

A FOUR-TERMINAL CURRENT SHUNT WITH CALCULABLE AC RESPONSE

O. B. Laug, T. M. Souders, and B. C. Waltrip

National Institute of Standards and Technology, Gaithersburg, MD 20899

ABSTRACT

The design of a 0.1 Ω, four-terminal current shunt with calculable frequency dependence up to 1 MHz is described. It is intended for use as a standard for current measurements up to 10 A rms with the primary purpose of being able to tie alternating-current measurements to direct-current measurements. The shunt is of the bifilar flat-strip configuration where the effects of self-inductance, skin effect, capacitance, dissipation factor, and eddy-current losses are considered. Contributions of the individual effects, where applicable, are determined by calculation based on geometry and corroborated by differential measurements and finite-element field simulations. The uncertainties due to dimensional and electrical measurement tolerances are computed as well.

In addition to the calculable aspects of the shunt this technical note provides assembly details of the shunt based on the mechanical drawings made available in the appendix. The practical issues of measuring 4-terminal shunts with emphasis on dealing with common-mode potentials are discussed. The thermal properties of the current shunt are presented together with some suggestions on reducing the power coefficient of resistance.

KEY WORDS: 0.1 ohm shunt, 4-terminal shunt, ac resistor, bifilar shunt, calculable shunt, current shunt

1. INTRODUCTION

The measurement or sensing of current is traditionally made using a low resistance current shunt, current transformer (CT), mutual inductor (Rogowski coil), or Hall Effect device. Each of these sensors has certain attributes which makes them useful for a given application. In support of the NIST calibration service which provides AC-DC Difference calibrations of thermal current converters and ac shunts up to 20 A and 100 kHz, our current shunt with calculable frequency response, is intended to be used as a working standard. Moreover, it can help serve in the buildup process from lower currents to establish uncertainties at higher levels of current. Another important electrical metrology application for accurate current determinations is the measurement of real and reactive power including higher order harmonics of current where the effects of phase angle become important.

Current Transformers (CTs) are widely used to scale a high-level primary current to a lower level secondary current. The secondary current can be measured directly with a calibrated thermal converter or as a voltage across a burden resistor. While CTs are limited in bandwidth and do not operate at dc (except for zero-flux designs), they offer superior isolation. Current shunts do not have the same inherent isolation properties. Thus, when measuring the characteristics of a four terminal current shunt special attention must be given to the rejection of common-mode voltages and loading at the potential terminals. These become critical measurement issues when a 4-terminal current shunt is compared against other current measuring devices.

Current shunts used for measuring ac currents require conductor configurations that are as noninductive as possible. The presence of inductance is the primary nemesis of a shunt resulting in appreciable phase angle errors, and to second order, magnitude errors. Cylindrical and bifilar flat strip designs can both give low inductance. However, the practical physical limitations of each of these configurations do not allow the design to go to the limit of zero inductance. The small but finite inductance of each design can be calculated, and the coaxial configuration has a closed-form solution. The usual arrangement for a coaxial design is to employ an inner tube of a given resistance material enclosed by an outer tube acting as the return path for the current that is launched at the end of the center tube. Coaxial designs tend to be difficult to fabricate in that the inner tube of resistance material must be as thin as possible to minimize skin-effect errors yet be self supporting. Some designs substitute a cage of fine parallel wires that serve as the inner tube. Another disadvantage of the coaxial design is the difficulty of transporting heat from the resistance element to the ambient. An air dielectric between the inner and outer tube is a poor conductor of heat. Some designs partially overcome the thermal problem by employing a liquid or paste dielectric with desirable thermal properties to fill the air space. Any significant power generated in the resistance element will cause a temperature rise depending on the thermal resistance to the ambient. Temperature changes in the resistance element will cause the shunt to display a power coefficient of resistance if the resistance material exhibits a non-zero temperature coefficient of resistance.

A bifilar strip configuration can also have low and calculable inductance provided that a high width-to-thickness aspect ratio of the resistance material is maintained. The bifilar configuration that we have chosen is shown in Fig. 1. The design has two main attributes; it is relatively simple to fabricate, and the thermal issues are easier to accommodate. A thin dielectric placed between the folded strip insulates the two halves preventing a short circuit along the intended path. Adding a thin dielectric between the strips increases the inductance slightly but its effects are still calculable. By clamping the folded element together with flat blocks insures mechanical stability of the structure. The blocks are made of aluminum with integral fins to provide a low thermal resistance path from the resistance element to the ambient. In our model a fan attached to the shunt provides forced cooling across the fins to further lower the thermal resistance from the aluminum blocks to the ambient.

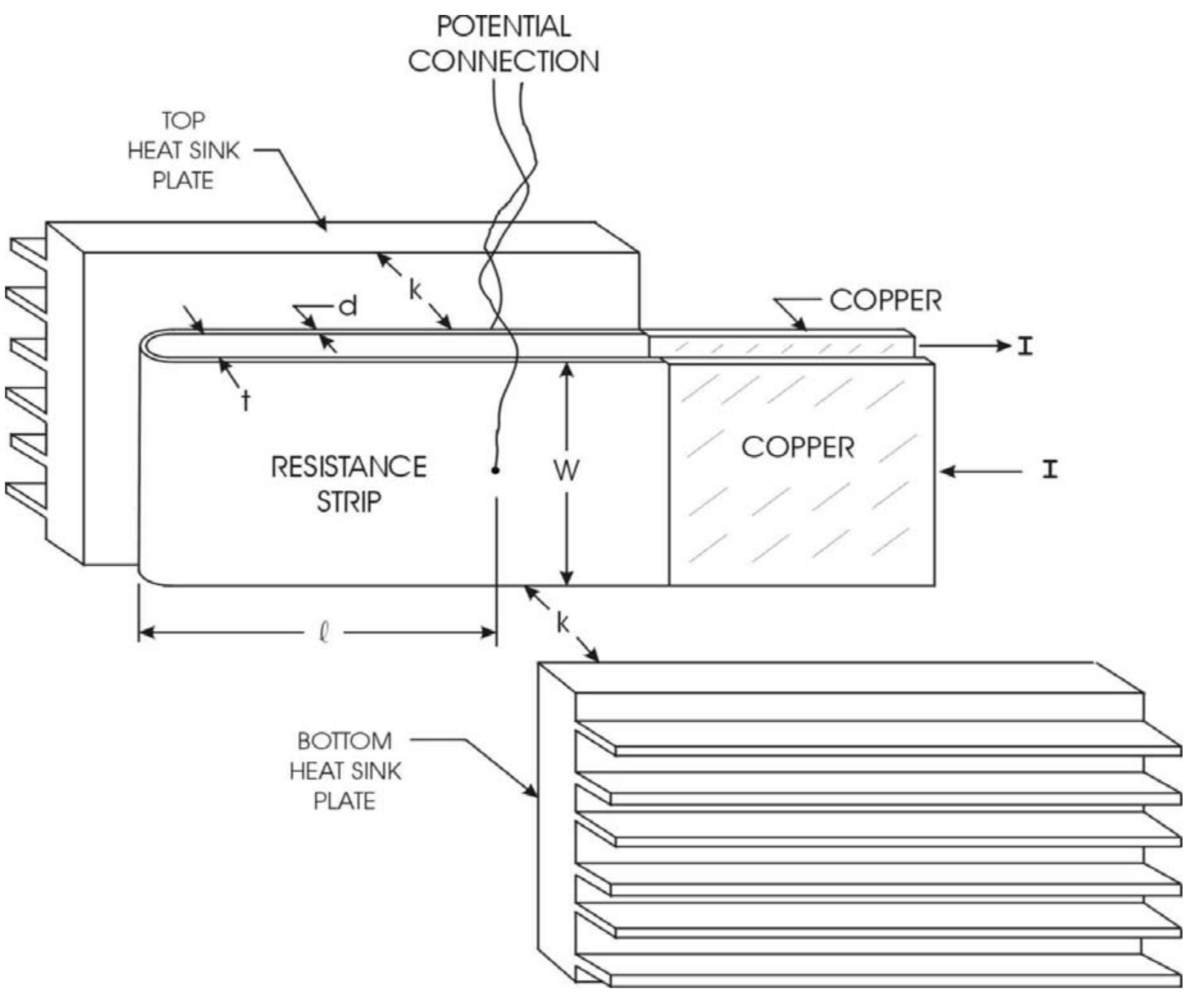

Figure 1. Basic diagram of the bifilar configuration

2. THE CALCULABLE AC RESPONSE

Calculations were performed to derive the complex frequency response of the bifilar shunt configuration of Fig. 1 based on applicable formulae and nominal dimensions taken from the prototype model designed for a nominal 0.1 Ω resistance. Contributions from equivalent inductance, inductive coupling to the aluminum heat sinks, shunt capacitance and dissipation factor, skin effect, and electro-thermal effects were all considered. Uncertainties due to dimensional and electrical measurement tolerances are computed as well. Four different configurations were studied, differing by the dielectric materials that were used to separate the halves of the resistance strip, and the dielectric used to separate the resistance strip from the heat sinks.

2.1 Inductance

Formulas for the inductance of 4-terminal bifilar strip resistors in terms of their dimensions were long ago derived by Silsbee [1]. These are presented as an expanded series in EQ (28) of that document. The relevant dimensions are expressed in cm. Using this formula, the equivalent series inductance of the resistor being fabricated has been calculated, and by differentiating with respect to the dimensional variables, the tolerances have been calculated as well. Ignoring the higher order terms (although second order terms were included in the actual calculations, reducing the value by about 0.5 %), the inductance is given by

$$L = \frac{4\pi\ell}{w}\left[t + \frac{2d}{3}\right]10^{-9} = 0.1460\ nH \tag{1}$$

where,

w	= width of strip	=	5.08 cm (2.00") nominal
d	= thickness of strip	=	0.00508 cm (0.002") nominal
t	= thickness of insulator	=	0.00254 cm (0.001") nominal
ℓ	= length of circuit	=	10.008 cm (3.94")

(Here the thickness, t, is given for the configuration finally chosen.)
The deviation in inductance resulting from dimensional deviations from nominal is given by

$$\Delta L = 16.5\,\Delta d - 0.0289\Delta w + 0.0147\Delta\ell + 24.8\Delta t \tag{2}$$

Since the width and length of the strip are relatively large (approximately 5 cm and 10 cm respectively), measurements of *w* and *l* can easily be made with 1 % uncertainty. The small dimensions (0.005 cm and 0.0025 cm) of d and t however have estimated 2 σ measurement uncertainties of about 15%. Taking the root-sum-of-squares of the four terms in (2), assuming 1 % tolerances for *w* and *l* and 15% for *d* and *t*, gives an 11 % uncertainty in *L*. The corresponding inductive time constant (L/R) and associated uncertainty are given by τ = 1.460 ns ± 0.16 ns.

2.2 Capacitance and Dielectric Loss

There are six components of shunt capacitance (and associated dielectric loss) that affect the frequency response of the resistor (see fig. 2): (C_1) the distributed capacitance between the two halves of the strip from the fold to the potential terminals; (C_2) the distributed capacitance between the two halves of the strip from the potential terminals to the termination with the current terminals; (C_3) the lumped capacitance between the current terminals; (C_4) the distributed capacitance between the strip and the lower heat sink from the fold to the lower potential terminal; (C_5) the distributed capacitance between the strip and the upper heat sink from the fold to the upper potential terminal; and (C_6) the distributed capacitance between the strip and the upper heat sink from the upper potential terminal to the end of the strip. Note that the aluminum heat sinks are connected to the lower current terminal. The values of each of these capacitances (and associated conductances) have been estimated from direct capacitance (and dissipation factor) measurements and knowledge of the dimensions of the structure.

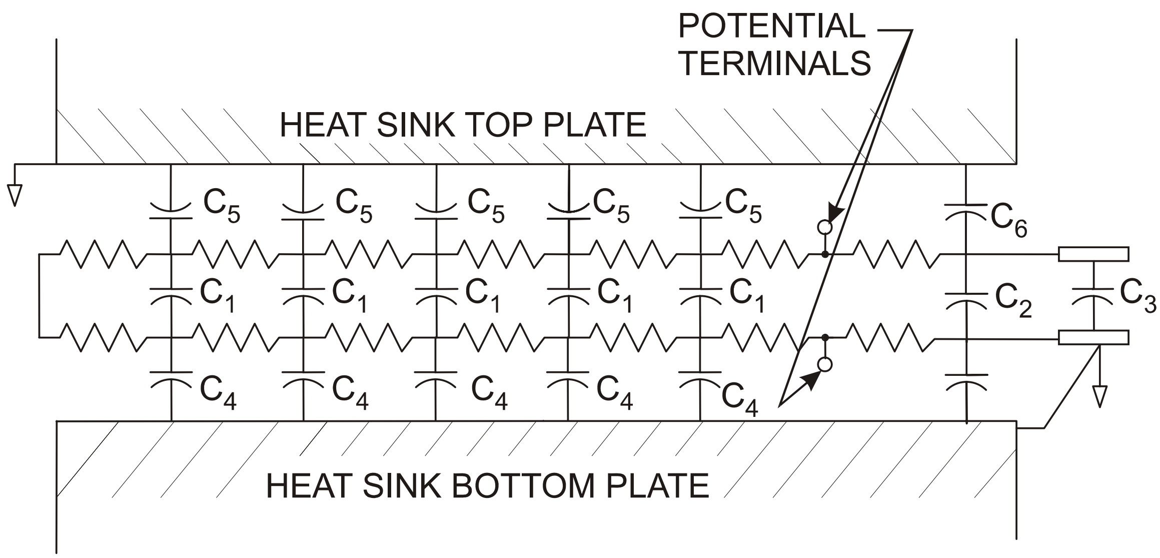

Figure 2. Model of distributed capacitances and associated dissipation factor

Table I
Measured Capacitances in nF, and (Conductances in µS) at 100 kHz

Dielectric Used ► / **Capacitance measured ▼**	**M2_M2**	**M2_R15**	**M1_M2**	**M1_R15**
$C_{e\text{-}e\_X}$ **Between Elements**	**2.30 (13.6)**	**2.30 (13.6)**	**4.34 (25.0)**	**4.34 (25.0)**
$C_{e\text{-}a\_Y}$ **Elements to Heat Sinks**	**4.67 (55.3)**	**0.98 (1.6)**	**4.67 (55.3)**	**0.98 (1.6)**
C_c, **Between I Terminals**	**0.49 (14.1)**	**0.49 (14.1)**	**0.49 (14.1)**	**0.49 (14.1)**
Capacitance derived ▼				
C_3	0.63 (18.1)	0.63 (18.1)	0.63 (18.1)	0.63 (18.1)
C_{1_M2}	0.67 (4.0)	0.67 (4.0)		
C_{2_M2}	0.31 (1.8)	0.31 (1.8)		
$C_{(4+5)\_M2}$	1.51 (17.9)		1.51 (17.9)	
C_{6_M2}	0.31 (3.6)		0.31 (3.6)	
$C_{(4+5)\_R15}$		0.32 (0.5)		0.32 (0.5)
C_{6_R15}		0.064 (0.1)		0.064 (0.1)
C_{1_M1}			1.27 (7.3)	1.27 (7.3)
C_{2_M1}			0.58 (3.3)	0.58 (3.3)

For each shunt configuration studied, measurements were made of the total capacitance, $C_{e\text{-}e\_X}$, between two equivalent resistor elements (strips) with the designated separation but not connected where the fold would normally occur, the total capacitance, $C_{e\text{-}a\_Y}$, between the resistance elements connected together and the two heat sinks connected together, and the total capacitance, C_c, between the two current terminals by themselves with no resistance elements connected. These measurements are reported in bold font in Table I, and the corresponding conductances are reported beneath them in parentheses, for four different dielectric configurations. At the top of each column is the configuration code for the dielectrics used. The left part of the configuration code designates the dielectric used between the resistance strips, with M1 and M2 designating 25.4 µm (1 mil) and 50.8 µm (2 mil) Mylar, respectively. The right part of the code designates the dielectric separating the heat sinks from the resistance strips, with M2 designating 50.8 µm (2 mil) Mylar, and R15 designating 381 µm (15 mil) thermally conductive rubber.

The equivalent effect of each of the six identified capacitances (and the associated conductances) is modeled by a lumped equivalent capacitance (or conductance) connected across the potential terminals, i.e., in parallel with the defined resistance. The lumped equivalent capacitances (and conductances) are computed in two steps, and the final values are listed in Table I in normal font. In the first step, the proportional amounts of the measured capacitances that contribute to each of the six components are computed as intermediate values, based on the dimensions of the strip from the fold to the potential terminals, and from the fold to the end of the strip. From these intermediate values, the equivalent lumped values are computed from integral equations that are based on the assumption that the capacitances, conductances and strip resistance are all uniformly distributed over the length of the resistance strip.

The lumped equivalent capacitances are computed from the following formulas, where ℓ_T is the total length of the resistance strip from fold to current terminal (11.43 cm), ℓ_P is the length of the strip from the fold to the potential terminal (10.01 cm), $\Delta\ell$ is the difference between ℓ_T and ℓ_P, *X* refers to the dielectric between resistance strips, and *Y* refers to the dielectric between resistor and heat sinks.

$$C_{1\_M2} \quad \text{and} \quad C_{1\_M1} = \left(C_{1\_X}\right)/3 \tag{3}$$

$$C_{2\_M2} \quad \text{and} \quad C_{2\_M1} = C_{2\_X}\left(1+\frac{\Delta\ell}{2\ell_P}\right) \tag{4}$$

$$C_3 = C_C\left(1+\frac{\Delta\ell}{\ell_P}\right) \tag{5}$$

$$C_{(4+5)\_M2} \quad \text{and} \quad C_{(4+5)\_R15} = \left(C_{4\_Y}+C_{5\_Y}\right)\left(\frac{1}{3}+\frac{\Delta\ell}{4\ell_P}\right) \tag{6}$$

$$C_{6\_M2} \quad \text{and} \quad C_{6\_R15} = C_{6\_Y}\left(1+\frac{3\Delta\ell}{8\,\ell_P}\right) \tag{7}$$

As noted above, these formulae were derived by determining the capacitances per unit length and then integrating the effects of the differential shunting currents over the length of the structure. It is assumed that in use the two heat sink plates are electrically connected together and are both connected to one of the current terminals. The intermediate capacitances C_{1_*} through C_{6_*} are defined as follows, based on the measured values in the table:

$$C_{1\_X} = \frac{\ell_P}{\ell_T}\times C_{e-e\_X} \tag{8}$$

Between the resistance strips from the fold to the potential terminals, for *X* dielectric

$$C_{2\_X} = \frac{\Delta\ell}{\ell_T} \times C_{e-e\_X} \quad \textbf{(9)}$$

Between the resistance strips from the potential terminals to the end, for *X* dielectric

$$C_{4\_Y} + C_{5\_Y} = \frac{\ell_P}{\ell_T} \times C_{e-a\_Y} \quad \textbf{(10)}$$

Between one resistance strip and heat sink, from the fold to the potential terminals, for *Y* dielectric

$$C_{6\_Y} = \frac{\Delta\ell}{\ell_T} \times \frac{C_{e-a\_Y}}{2} \quad \textbf{(11)}$$

Between one resistance strip and heat sink, from the potential terminals to the end, for *Y* dielectric

The capacitive contributions to the phase angle of the respective shunt geometries are computed from the values in Table I as:

$$\Phi_C = -2\pi f\Big((C_{1\_XX}) + (C_{2\_XX}) + (C_3) + (C_{(4+5)\_YY}) + (C_{6\_YY})\Big)R \qquad \textbf{(12)}$$

where *f* is frequency, *R* is resistance (0.1 Ω) and *XX* and *YY* refer to the appropriate dielectric (between resistance strips and between strips and heat sinks, respectively) for the geometry in question. Using the average values from Table I in (12), we get the capacitive time constants given in Table II for the four configurations.

Table II
Calculated Capacitive Time Constants and Resistance Change due to Dielectric Loss

	M2_M2	M2_R15	M1_M2	M1_R15
Time Constant (ns)	0.342	0.199	0.429	0.285
Uncertainty (ns)	0.032	0.018	0.040	0.030
$(R_{ac} - R_{dc})/R_{dc}$ (μΩ/Ω/kHz)	-0.045	-0.024	-0.050	-0.029
Uncertainty (μΩ/Ω/kHz)	0.007	0.005	0.007	0.005

Assuming that the uncertainties in the five capacitances of (12) are within 15% (2 σ) and recognizing that the uncertainties of the first two terms are directly correlated as are the last two terms, we obtain the expanded uncertainties in the values of time constants shown in the table. Here the sum of the first two terms is root-sum-squared with third term and the sum of the last two terms to give the expanded uncertainties.

The equivalent shunt conductances were computed from the components of measured conductance using equations (3) through (11), substituting "G" for "C". The total proportional change in resistance with frequency caused by the shunting conductances is given by:

$$\frac{(R_{ac} - R_{dc})}{R_{dc}} = -0.01f\big((G_{1\_XX}) + (G_{2\_XX}) + (G_3) + (G_{(4+5)\_YY}) + (G_{6\_YY})\big)R \tag{13}$$

where f is the operating frequency in kHz (since the conductances of Table I are for 100 kHz). Using the average values from Table I in (13), we get the proportional changes in resistance given in Table II for the four configurations. The expanded uncertainties (2 σ) for these values are computed as for the time constant case, assuming the uncertainties in the conductance measurements to be ± 25 %. The resulting uncertainties are less than 1 μΩ/Ω for each of the configurations at frequencies up to 100 kHz.

2.3 Skin Effect

The change in resistance due to skin effect is estimated to be less than 1 μΩ/Ω at 100 kHz. In [2], Silsbee gives two equations for the skin effect of parallel plate resistors. The first (EQ20, p. 86) assumes the strips are so wide that edge effects are negligible. For the shunt in question (with d = 0.00508 cm, w = 5.08 cm, ρ = 1.295 x 10^2 μΩ-cm for Evanohm, and a relative permeability of 1 for Evanohm), this gives a ratio of ac resistance (*R'*) to dc resistance (*R*) of

$$\frac{R'}{R} = 1 + 5.5 \times 10^{-9} \quad \text{at } f = 100\,\text{kHz} \tag{14}$$

The second equation (EQ21, p. 86) assumes the plates are so far apart that they exert no effect on each other and therefore current crowding at the edges is appreciable. This gives

$$\frac{R'}{R} = 1 + 2.17 \times 10^{-2} \quad \text{at } f = 100\,\text{kHz} \tag{15}$$

While one can easily conclude from the subsequent discussion in Silsbee that our case is closer to the first result, it is hard to quantify by how much. It is clear however, that the skin effect at the frequencies of interest here (e.g., below 10 MHz) should be directly proportional to f^2 and inversely proportional to ρ^2. To get a better estimate of the skin effect for our case, the structure was modeled using a finite element field modeling software program [3]. The results for configurations with 25.4 μm (1 mil) separation between the resistance strips are given in Table III where R_f - R_{1k} is the resistance change from 1 kHz to frequency *f*. The resistance change for the 50.8 μm (2 mil) separation is essentially the same. Higher frequencies were chosen for the simulation to improve resolution and accuracy. These results indicate a skin effect about 10 times larger than that given in (14) (although much less than that given in (15)), and show a nearly square-law dependence on frequency, both of which are consistent with Silsbee's observations.

Table III
Skin Effect vs. Frequency

f (MHz)	0.001	0.1	1.0	2.0	5.0	10
$(R_f - R_{1k})/ R_f$ μΩ/Ω	0	0	5	22	138	554

2.4 Eddy Current Losses

To quantify the effective resistance change caused by eddy current losses in the aluminum heat sinks, additional simulations were performed using the field modeling software [3] noted previously. Simulations were run for the four different combinations of separation between strips, *t*, and separation, *k*, between the resistance strip and heat sink plates. These results are summarized in Table IV. As before, in the configuration designations at the tops of the columns, the first number designates the separation between the resistance strips (x 25.4 μm, i.e., in mils) and the second number designates the separation between the resistance strip and the heat sink (x 25.4 μm). The letters designate the dielectric materials used, although for these simulations that information was not needed since the separation was assumed to be free space. Note that the frequency range used for these simulations is ten times higher than that used for the measurements discussed in the next section.

Table IV
Resistance Change relative to DC Due to Eddy Current Losses in Heat Sinks

FREQ. kHz	**M2_M2** μΩ/Ω	**M2_R15** μΩ/Ω	**M1_M2** μΩ/Ω	**M1_R15** μΩ/Ω
1	0.071	0.055	0.018	0.014
2	0.198	0.139	0.049	0.035
5	0.752	0.437	0.190	0.111
10	2.02	0.972	0.518	0.250
20	5.31	2.02	1.384	0.523
50	18.2	4.78	4.86	1.250
100	43.8	8.48	11.21	2.232
200	100.0	14.23	28.29	3.79
500	271	26.6	80.16	7.09
1000	533	40.8	163.0	11.06

For the two configurations with separation *k* of 50.8 μm (2 mils) designated M2, the resistance change is approximately proportional to f^{1} over the frequency range considered.

However, for the configurations using R15 (k of 381 μm (15 mils)), the dependence on frequency decreases to approximately $f^{0.67}$. As seen in the table, the resistance change is quite small for the M1_R15 configuration that we have chosen to use, giving 2 μΩ/Ω at 100 kHz and only 11 μΩ/Ω at 1 MHz.

2.5 Thermoelectric Effects

The thermoelectric properties of resistive alloys can give rise to an apparent change in the dc resistance of resistors made from them [4]. This takes place as follows: The current passing through junctions of dissimilar metals in the resistor (e.g., at the current terminals) gives rise to a difference in temperatures at the two junctions due to the Peltier effect. The temperature difference in turn creates opposing thermoelectric voltages in the junctions via the Seebeck effect and the net result is an increase in the apparent resistance. If the current is reversed, the temperature difference reverses so the thermoelectric voltage reverses also with the consequence that averaging with reversals is unable to eliminate the effect. However, as the rate of reversal exceeds the reciprocal of the thermal time constants of the structure, the effect disappears because there is no opportunity for a temperature difference to be established between the junctions. This effect is mitigated in the resistor design in question as follows: The Seebeck coefficient for Evanohm is relatively close to that of copper, so that the thermoelectric potential is less than 2.5 μV/ºC. Since the Peltier coefficient is directly proportional to the Seebeck coefficient, the rate of heat generation/absorption at the junctions is also very small. The two copper plates that form the current terminals have relatively low thermal resistance between them since they are separated by only 0.08 cm of Bakelite sheet and the communicating area of the plates is approximately 39 cm^2; consequently the temperature difference between the two plates should be very small, especially since the rate of heat production is low. In our four-terminal design however, the salient thermoelectric voltages are those at the junctions of the resistance strip with the potential leads, rather than those at the current terminals. The temperature difference at these junctions caused by the Peltier heating/cooling of the current terminals should be much smaller still. These junctions are each separated from the heat-producing junctions by approximately 1.4 cm of Evanohm strip that has a cross-sectional area of only 0.026 cm, allowing only very slow heat conduction. Furthermore, the two strips (at either ends of the resistor) are in very close thermal contact over the full 1.4 cm path of thermal conduction, being separated by only 0.0025 cm of Mylar insulation. Based on these considerations, we believe the temperature difference at the junctions of the potential terminals (caused by Peltier heat/cooling at the junctions of the current terminals) will be less than 0.01ºC for currents up to 10 A. This temperature difference will cause a thermoelectric potential of less than 0.025 μV in each junction, changing the apparent resistance by no more than 0.05 μΩ/Ω. The effect is thus considered negligibly small.

4. EXPERIMENTAL AC MEASUREMENTS

In an attempt to corroborate the above calculations and simulation results, we have made a series of measurements. While there are currently no impedance standards or methods of intercomparison available at NIST that can be used to independently verify the calculations mentioned above, the calculations can be corroborated or bounded using differential measurements in which the dimensions and materials of construction are changed. Thus, a series of experiments was performed in which the calculable shunts were intercompared with transformer-scaled shunts having the same nominal (0.1 Ω) value, in a bridge circuit with dual sampling channels. A circuit originally developed for testing phase angle generators was used as a magnitude and phase comparator and is diagramed in Fig. 3. Data from the samplers is used to compute the magnitude and phase (relative to the synchronous trigger) of the two channels. From this information, the relative magnitude and phase differences between the two channels are calculated. Although not important for differential measurements, the two channels are repeatedly swapped and the results averaged to eliminate channel-to-channel differences in the sampler. The transformer-scaled shunt acts as a dummy standard, and is only required to have stable frequency response from test to test. The primary-to-secondary circuit isolation provided by the transformer allows the two devices to be connected in series (i.e., primary of transformer in series with resistive shunt) while simultaneously grounding one potential terminal of each device. Errors caused by shunt capacitance from primary circuit to secondary and primary circuit to ground must be considered if this method is relied upon for accurate intercomparison data, but for the differential measurements of interest here, such errors are inconsequential.

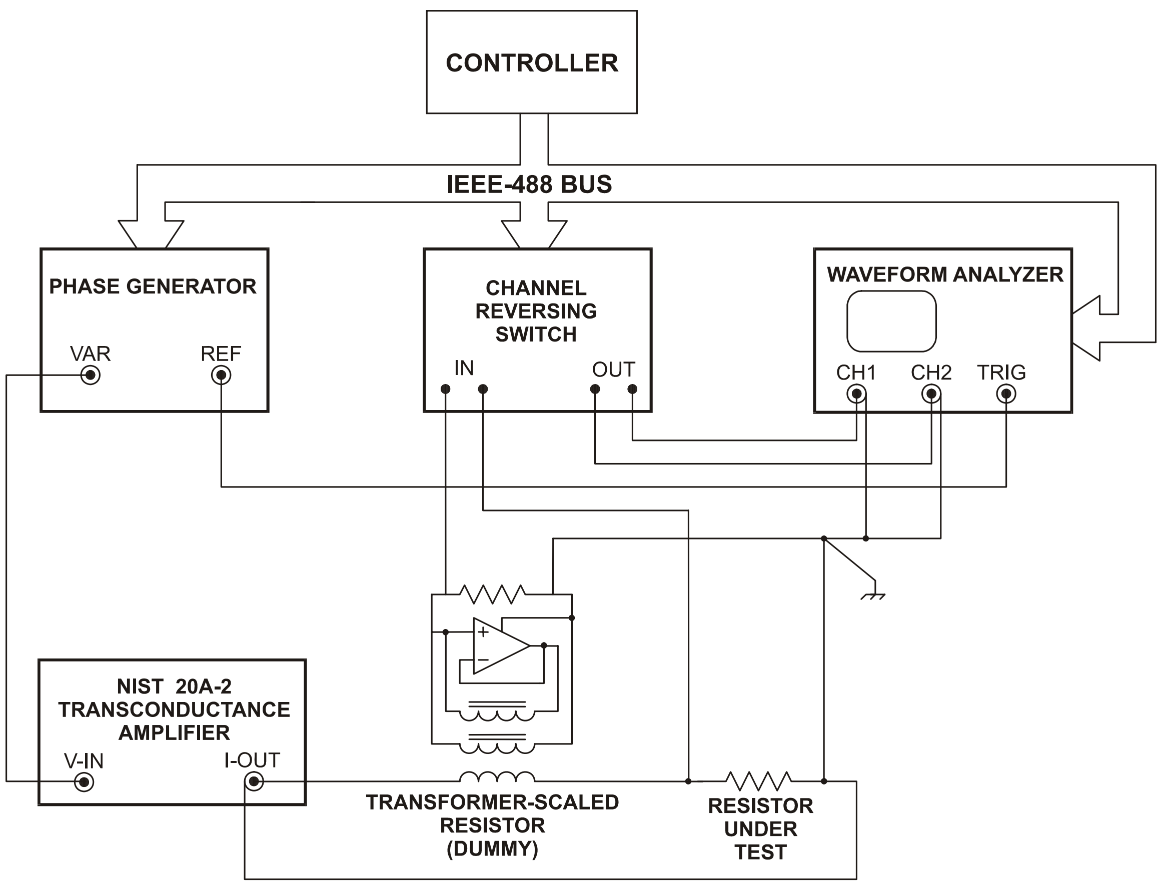

Figure 3. Basic comparator system

Table V
Bridge Comparison Data: Resistor Configuration vs. Transformer Scaled Resistor
Proportional Magnitude and Phase Differences

FREQ. kHz	**M2_M2** x 10^{-5}	μRad	**M2_R15** x 10^{-5}	μRad	**M1_M2** x 10^{-5}	μRad	**M1_R15** x 10^{-5}	μRad
0.1	1050	55.8	1038	59.3	1089	61.1	1003	61.1
0.2	1059	29.7	1037	26.2	1088	33.2	1009	31.4
0.5	1066	12.2	1036	10.5	1085	14.0	1012	12.2
1.0	1066	7.0	1036	3.5	1082	8.7	1016	10.5
2.0	1066	0	1030	-5.2	1078	7.0	1013	5.2
5.0	1064	-19.2	1028	-20.9	1074	5.2	1013	0
10	1068	-45.4	1027	-54.1	1075	0	1010	-8.7
20	1067	-96.0	1022	-110	1073	-10.5	1008	-27.9
50	1059	-251.3	1010	-296.7	1057	-36.7	997	-87.3
100	1331	-649.3	1272	-754.0	1321	-233.9	1253	-347.3

Data acquired using this measurement system are presented in Table V for the four different shunt configurations involving 25.4 μm (1 mil) or 50.8 μm (2 mil) Mylar dielectric between the resistance strips, and 50.8 μm (2 mil) Mylar or 381 μm (15 mil) thermally conductive rubber between the resistance strips and heat sink plates.

Because the uncertainties in the reference transformer-scaled shunt are much larger than the uncertainties we are seeking for the calculable shunts, we are only able to use measurement differences between configurations as a meaningful basis for comparison with calculations. Such comparisons are given in figs. 4-9 for phase angle differences, and in figs. 10-15 for resistance changes. These are further described below.

The major source of uncertainty in the differential responses derived from this data is the temperature coefficient of resistance of the shunt itself, which is approximately 20μΩ/Ω/ºC. We estimate that self-heating and room temperature changes contribute errors of up to 15 μΩ/Ω (k=2) in the differential magnitude responses that were derived from the data. In addition, we observed that the dc resistance of the shunt shifted each time the configuration was changed. We attribute this to stress-induced changes, and ignored resulting global offsets in the differential responses, as noted below. On the other hand, the differential phase angles are unaffected by temperature and stress to first order, and the errors in differential phase are dominated by type A uncertainties which are estimated to be 5 μrad for this data (for k=2), at all frequencies. Although data was obtained at frequencies down to 100 Hz, any differential changes in magnitude and phase below 1 kHz are totally overwhelmed by the measurement uncertainties. Therefore the results at frequencies below 1 kHz are ignored in the following sections.

3.1 Phase Comparisons

The measured phase differences between configuration pairs are presented in figs. 4-9 for the six unique pairs, along with the corresponding calculated phase differences based on the inductive and capacitive phase contributions discussed in sections 2.1 and 2.2 above. The error (meas. - calc.) is also given. "Calc." refers to the combined inductive and capacitive components. The largest error among these six plots is -54 µrad, occurring at 100 kHz for the (M2_M2)-(M1_R15) pair. In comparison, the absolute phase angle computed for the (M2_M2) condition is 1094 µrad, and that computed for the (M1_R15) condition is 738 µrad. Note that the level of agreement is well within the uncertainties expected for the calculations (q.v., 101 µrad for M1_R15) based on the root-sum-squares of the uncertainties in *L* and *C*, as discussed in previous sections. These results also show that the phase differences are linear with frequency to well within the uncertainties of the measurement data.

3.2 Magnitude Comparisons

The measured resistance differences between configuration pairs are presented in figs. 10-15, along with the calculated resistance differences based on the dissipation errors given in Table II and the field simulations presented in Table IV for eddy current losses in the heat sinks. (At the frequencies for which measurement data are available, the calculated changes due to skin effect are negligible, per Table III.) To account for the dc offsets noted above, the measured differences are always normalized to the 1 kHz values. The difference (Meas. - Calc.) is also given.

Among all six configuration pairs, the largest difference between measured and calculated differences was $12 \cdot 10^{-6}$, which is less than the $15 \cdot 10^{-6}$ estimated uncertainty for the measurements. In the three cases where the calculated differences are greater than the estimated measurement uncertainty (i.e., the pairs involving the M2_M2 configuration), the agreement is relatively good between the measured and calculated values

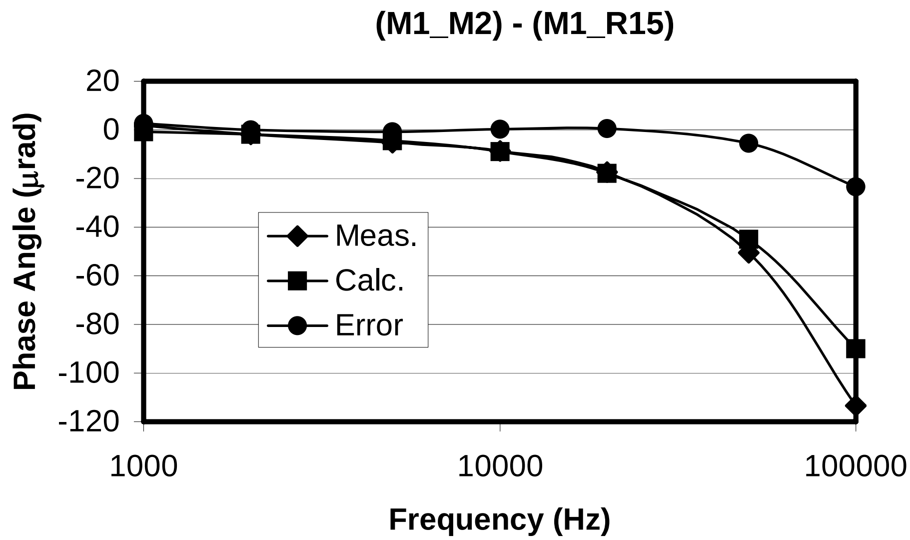

Figure 4. Measured phase difference between arrangements M1_M2 and M1_R15

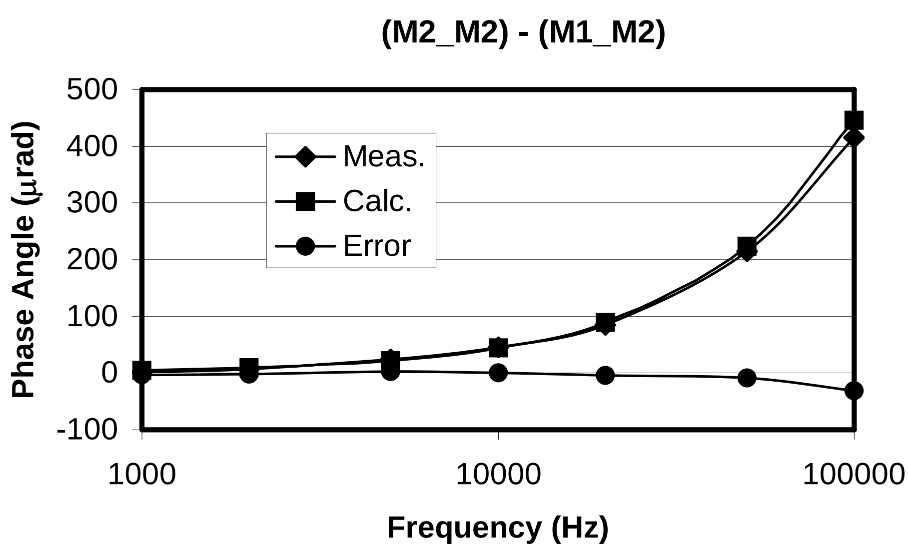

Figure 5. Measured phase difference between arrangements M2_M2 and M1_M2

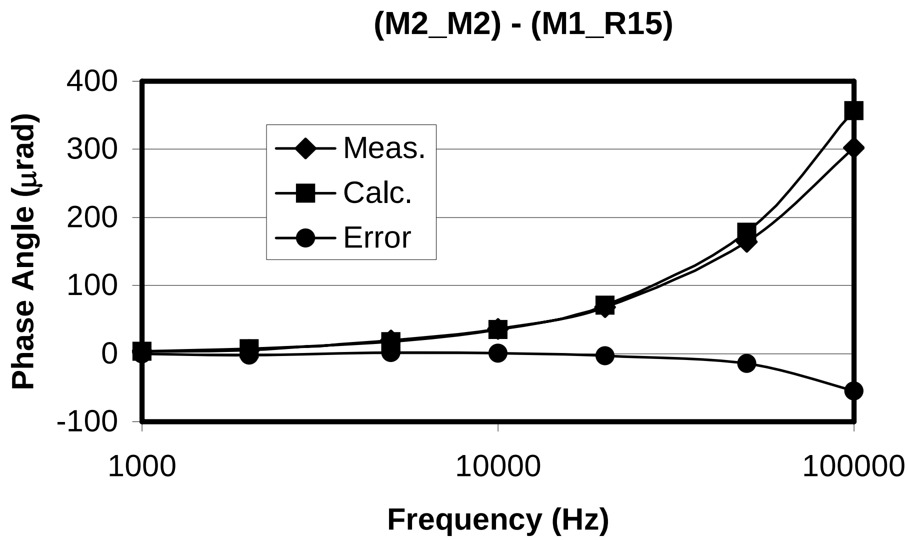

Figure 6. Measured phase difference between arrangements M2_M2 and M1_R15

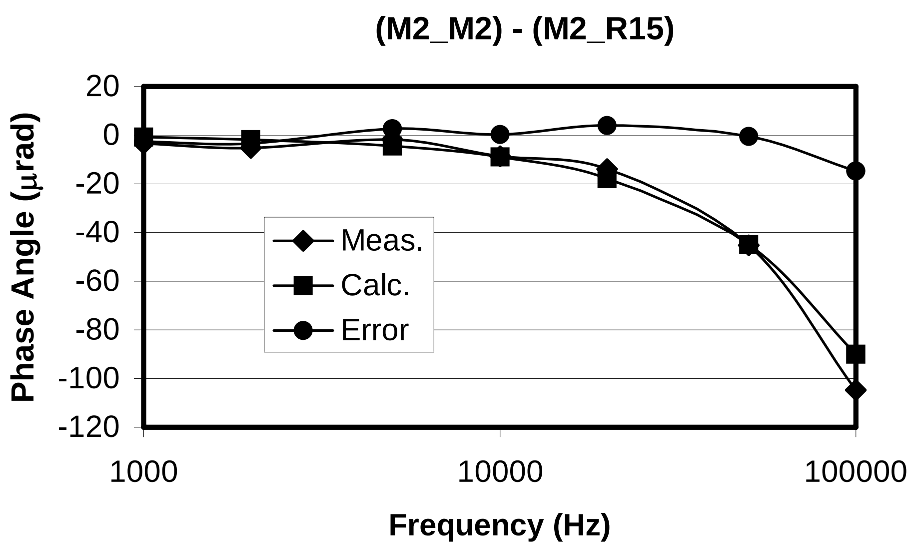

Figure 7. Measured phase difference between arrangements M2_M2 and M2_R15

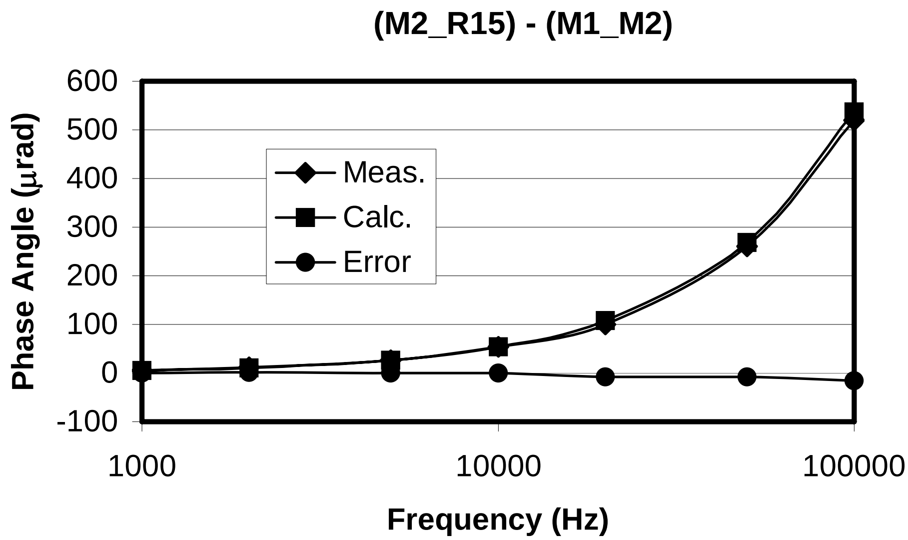

Figure 8. Measured phase difference between arrangements M2_R15 and M1_M2

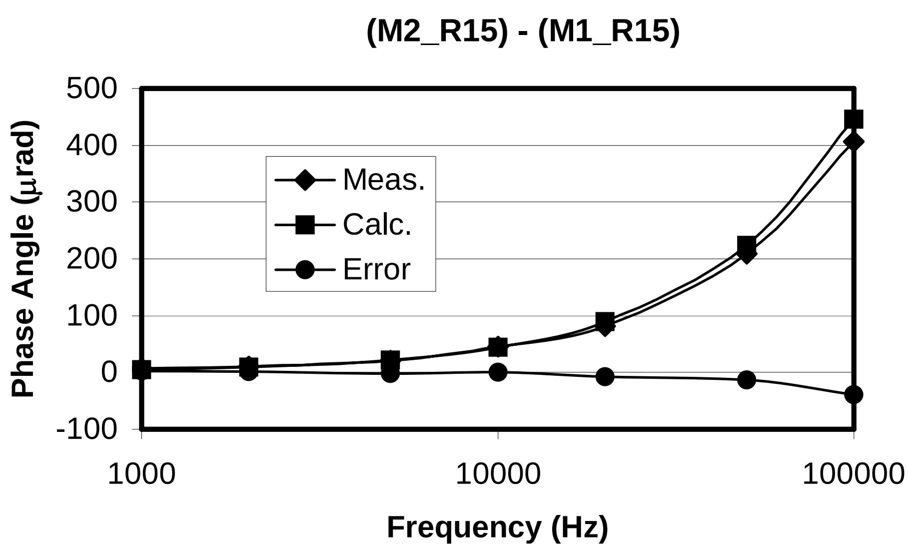

Figure 9. Measured phase difference between arrangements M2_R15 and M1_R15

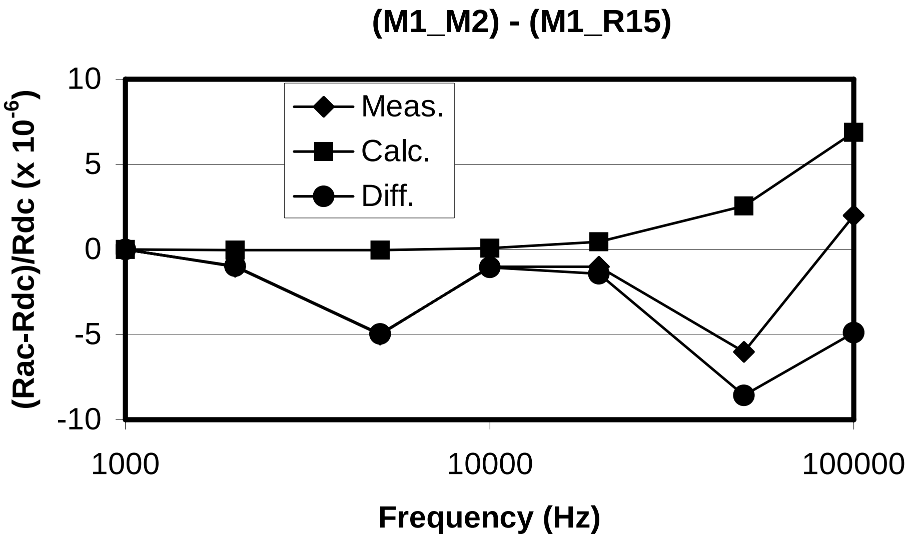

Figure 10. Measured resistance difference between arrangements M1_M2 and M1_R15

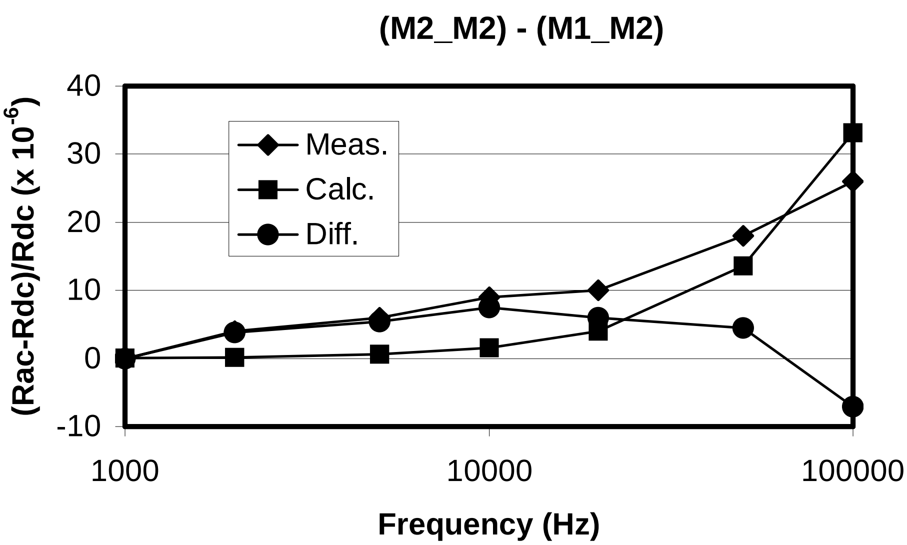

Figure 11. Measured resistance difference between arrangements M2_M2 and M1_M2

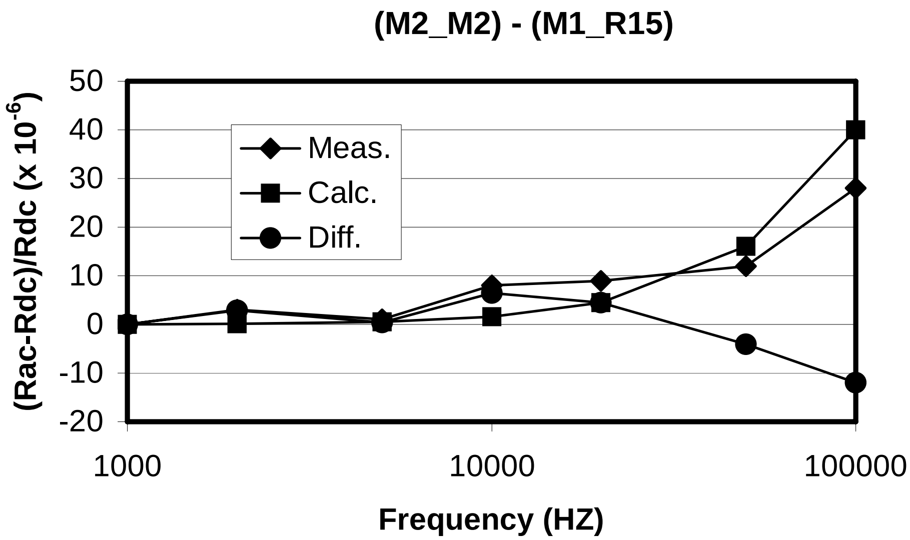

Figure 12. Measured resistance difference between arrangements M2_M2 and M1_R15

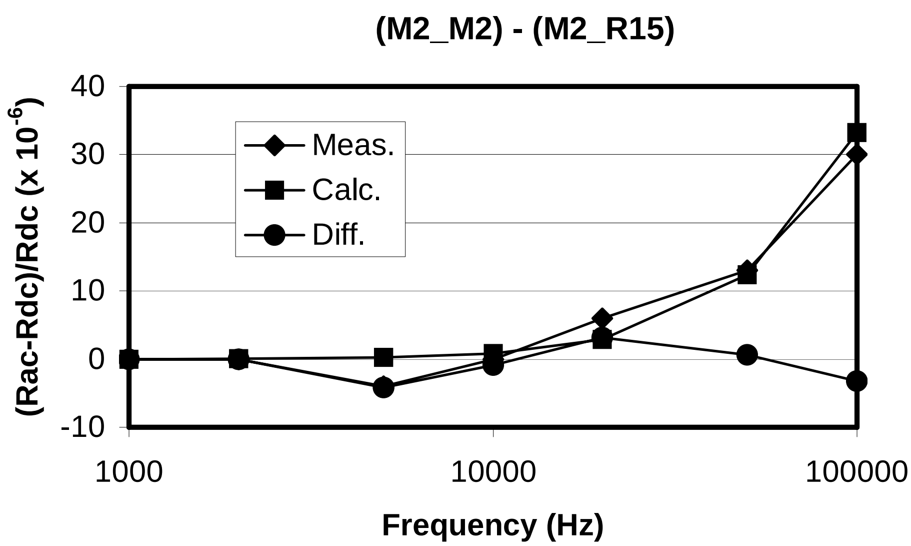

Figure 13. Measured resistance difference between arrangements M2_M2 and M2_R15

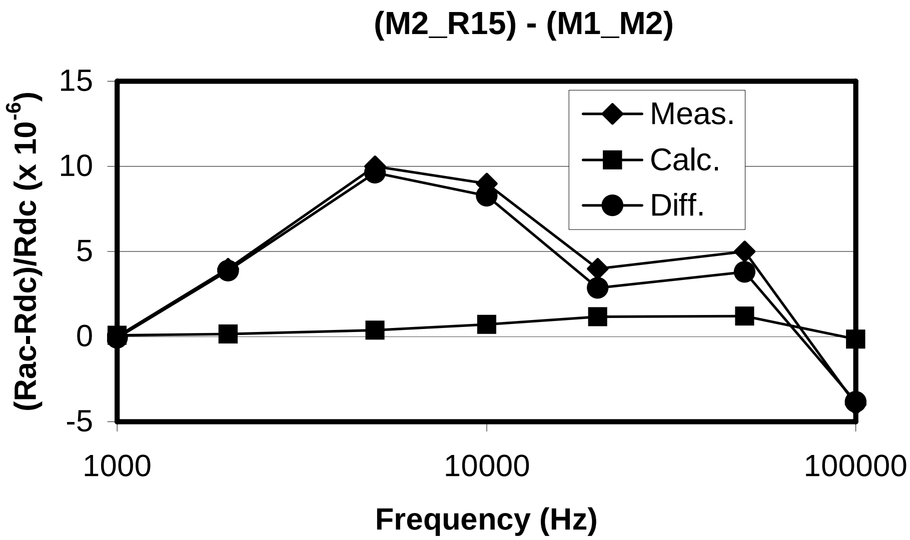

Figure 14. Measured resistance difference between arrangements M2_R15 and M1_M2

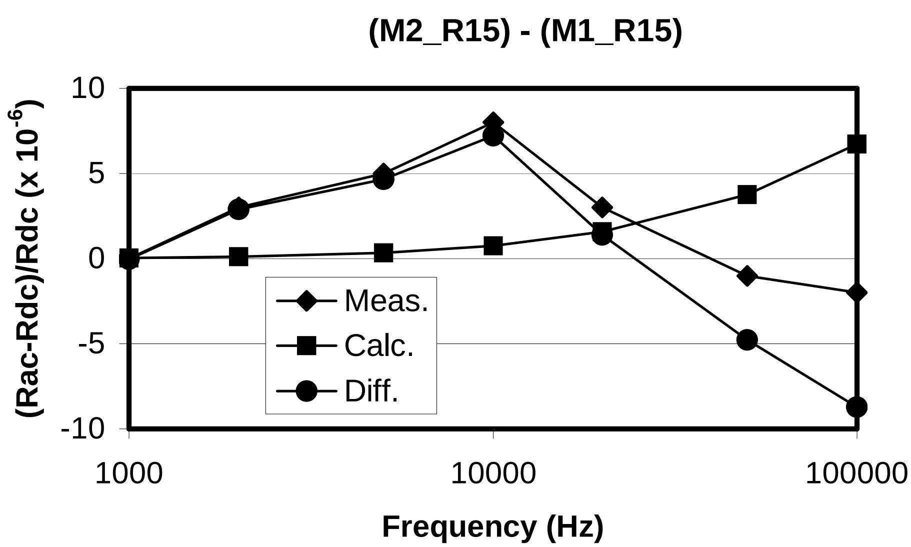

Figure 15. Measured resistance difference between arrangements M2_R15 and M1_R15

4. FINAL MAGNITUDE AND PHASE RESULTS

In summary, the experimental measurement results presented in the previous section are fully consistent with the calculated magnitude and phase responses, to within the estimated uncertainties of the measurement process.

The differential phase measurements agree with calculations to well within the estimated uncertainties of the calculations. Although there is likely a phase angle component caused by the eddy currents in the heat sink, it should be of the same order as the in-phase component (see Table IV) and consequently should be negligible compared to the uncertainties in the phase angle calculations.

Therefore, with a coverage factor of 2, the time constant of the M1_R15 configuration is assumed to be essentially constant up to 1 MHz, and is given by:

$$\tau = \tau_L - \tau_C \pm \left[(\Delta\tau_L)^2 + (\Delta\tau_C)^2 \right]^{1/2} = 1.17\,\text{ns} \pm 0.16\,\text{ns}. \qquad \textbf{(16)}$$

Over the frequency range of interest (0 - 1 MHz), the proportional change in resistance due to dielectric losses is given by

$$\Delta R_D \approx -2.9 \times 10^{-11} f\,. \qquad \textbf{(17)}$$

The calculated change in resistance due to skin effect for the M1_R15 configuration is closely approximated by

$$\Delta R_S \approx 5.5 \times 10^{-6} \left(\frac{f}{10^6} \right)^2, \qquad \textbf{(18)}$$

and the proportional change in resistance due to the calculated eddy current losses is approximated (to better than 0.27 μΩ/Ω) by:

$$\Delta R_E \approx 10^{-9} \times f^{0.674} \qquad \textbf{(19)}$$

where in each case f is the frequency in Hz. Based on the agreement between calculations and measurements for the resistive component, an uncertainty (with coverage factor of 2) can be assigned given by:

$$U_R \approx 10^{-6} + 1.5 \times 10^{-4} \times \frac{f}{10^6}\,. \qquad \textbf{(20)}$$

Therefore, over the frequency range of 0 - 1 MHz, the resistance of the M1_R15 configuration is given by :

$$R = R_{dc}\left[1 + 5.5\cdot 10^{-6}\left(\frac{f}{10^6}\right)^2 + 10^{-9}\times f^{0.674} - 2.9\times 10^{-11} f \pm\left(10^{-6} + 1.5\cdot 10^{-4}\times\left(\frac{f}{10^6}\right)\right)\right] \quad \textbf{(21)}$$

where R_{dc} is the dc resistance and f is the frequency in Hz.

The predicted resistance change (21) and phase angle, $\omega\tau$, (16) are plotted in figs. 16 and 17 over the frequency range from 1 kHz to 1 MHz, along with the corresponding uncertainty bounds.

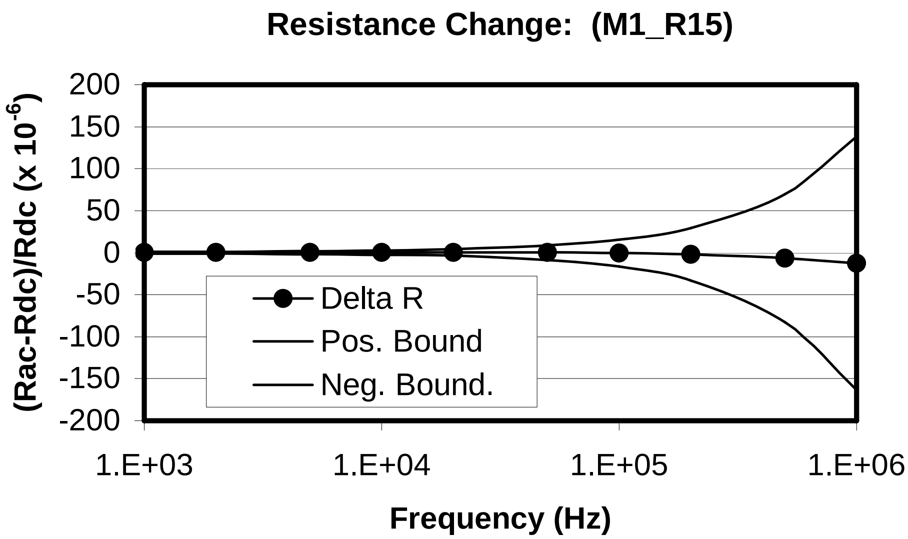

Figure 16. Calculated resistance vs. frequency for the selected arrangement M1_R15 with uncertainty bounds (k=2)

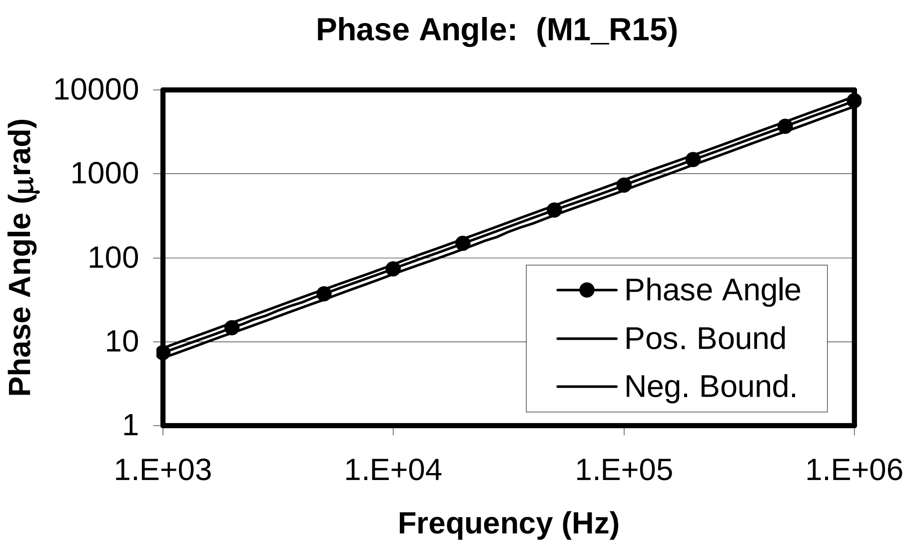

Figure 17. Calculated phase vs. frequency for the selected arrangement M1_R15 with uncertainty bounds (k=2)

5. CONSTRUCTION DETAILS

The following construction details are intended as a recipe for those readers interested in replicating the shunt from the mechanical drawings provided in Appendix A. The details were developed from numerous trial and error procedures and are coupled with an emphasis of important particulars that should be adhered to for those desiring to employ the basic design with modifications.

5.1 Preparing the bifilar resistance element

The material selected for the resistance element is from a metallic resistance alloy called Evanohm which is available on a roll as a thin strip 0.00508 cm thick and 5.08 cm wide having a nominal sheet resistivity, 0.025Ω/square of surface area. Thus, a nominal resistance of 0.1 Ω will require a length to width ratio of 4 which in this case results in a circuit length of about 20 cm. Note that the actual physical length of the circuit is twice the value defined in (1).

Cut a length of resistance strip equal to about 30 cm to provide for additional length from the potential terminals and the attachment edge of the current terminals. Place the sample in a brake and form a 90^0 bend at about 15 cm from one end. An alternate to using a brake is to form the initial bend by bending the material over the edge of a block of aluminum. Make sure that the bend is exactly orthogonal to the edge of the strip. Remove the strip from the brake and fold by hand the material back on itself while insuring that the edges of the folded strip are parallel. Flatten the fold as much as possible by rubbing stiff paper back and forth across the fold by hand while insuring the fold appears uniform across the width of the material. The material is malleable enough so that a tight fold can be formed entirely by hand without resorting to additional mechanical force. The objective in forming the shape of the fold is that it be reasonably compressed but still allow for a thin dielectric material to be positioned between the sheets up to and against the inside of the fold.

5.2 Tinning the strip for the current terminals

The next step is to trim the ends of the folded sample to a total length of 12.7 cm from the fold using a shear. An ordinary paper shear works well in this case. Place a tape mask across the width of the strip to expose 0.8 cm of resistance material from both sheared ends on the outsides of the folded strip. Use a high temperature masking tape such as Teflon to withstand soft-solder melting temperatures. Tin the unmasked ends across the width of the strip on each side using a flux intended for stainless steel. The most controlled process of tinning was done by heating each end of the strip on a hot plate while scrubbing the surface with flux and solder. Once the Evanohm material is wetted wipe off the excess leaving only a thin coating of solder.

5.3 Locating the potential terminal target points

The target points for the potential terminals are located midway across the width on each side of the bifilar strip at a determined distance from the fold to set the nominal resistance at 0.1Ω. A special jig was designed to locate the target points (see Fig. 18). The jig basically consists of a slot in a Bakelite material that can accept and clamp the folded strip of Evanohm material. Two pointed-tip screws threaded in the Bakelite can be turned to protrude against each side of the folded resistance element. A thin dielectric material such as 0.002” Mylar is placed between the folded sheet. A four-terminal resistance measurement is made by attaching current leads to the previously tinned ends of the strip, and connecting the sense leads to the threaded screws. It is important that the current leads are attached in a manner such that the current is applied across the entire width of the strip. A simple modification to an alligator clip can accomplish this by soldering two wide copper strips equal to the width of the strip to each jaw.

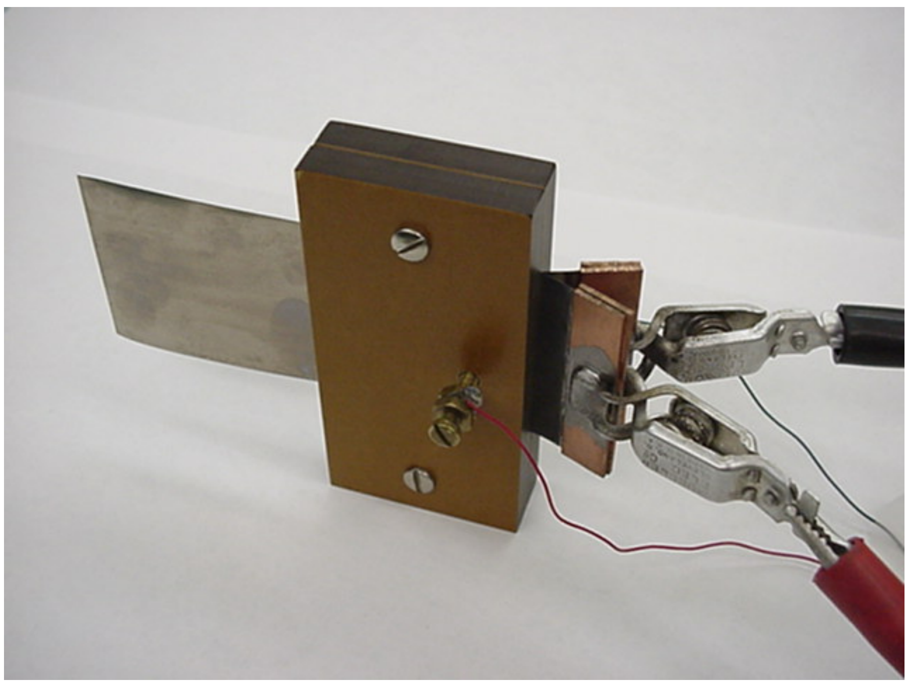

Fig. 18. Photograph of jig used to locate target points for potential terminals

Use a four-wire resistance-measuring instrument that has at least a 100 μΩ/Ω resolution with a provision for compensating the effects of thermally generated offset voltages. Monitor the resistance while lightly turning each screw to make contact to the strip. Through an iterative process of loosening the screws and sliding the strip to a new position and then retightening the screws again, it is possible to locate the point that provides the desired resistance. Once the desired position has been obtained, lightly tighten each of the screws to create a small dimple on each side of the resistance strip. Do not over tighten, as the objective is to create only very small visible indentions that become the two target locations where the potential leads will be attached.

5.4 Attaching the potential leads

Attaching the potential leads to the target points on the Evanohm strip is perhaps the most difficult and tedious part of the assembly process. Failure in the attachment process may ruin the bifilar strip, requiring another prepared strip. The method chosen is to spot-weld the end of # 30 copper Formvar-coated wire directly to the element. A commercially available capacitive discharge welder was chosen for this application having a 5 to 50 Watt-Second stored energy capacity. This type of welder commonly uses the capacitor discharge technique where the voltage stored on a capacitor is discharged through the circuit creating enough heat at the junction to fuse the metals together. A variable control sets the voltage on the capacitor, which establishes the potential energy at the weld site. Experimentation is required to determine the correct amount of energy. Too high a level will burn a hole through the resistance sheet while too little results in an incomplete attachment. The most reliable visible indicator of a good weld is a small ring of discoloration on the resistance sheet where the weld is formed. If the weld is sound the wire should be able to be moved back and forth at a slight angle without becoming detached.

It is necessary to first prepare the ends of the wires that will be welded to the resistance strip. Shear the end of the wire to form a flat surface that is at a right angle to the wire length. Depending on the type of shear it is usually necessary to dress the end of the wire with an abrasive to create a flat end. Experience has shown that the most reliable welds are formed if the end of the wire is held against the resistance strip with a jig that holds the wire and exerts downward pressure against the strip. The setup used to accomplish this was to employ a circuit probe micromanipulator with a 3-axis variable adjustment. The manipulator was adapted with a syringe needle to contain the wire. The beveled point of the needle was cut off. Fig. 19 shows the setup used to hold the wire and position it over the target point. The wire is positioned and locked about 1mm beyond the tip of the syringe needle. Note that an aluminum plate is placed under the sheet where the weld is performed. Having a back-up plate that acts as a heat sink was found to produce the most consistent results. The manipulator is spring-loaded in the Z direction so that once the X-Y position has been set above the target point the Z-axis control is moved until the spring in the manipulator is engaged and the butt end of the wire is forced against the Evanohm material with constant pressure. One connection of the welder is made to the wire and the other to the resistance strip. A discharge switch on the welder produces the one-shot pulse of energy. If the weld results in improper attachment of the lead it may be possible to try again, but if a hole is burned through the material it will be necessary to start over with another sample of material. It is advisable to first practice the technique on scrap material until the correct amount of energy has been determined. If a successful weld is achieved a small spot of fast-curing epoxy is applied around the weld area. Once the epoxy has cured the wire is bent down against the strip and held in place with epoxy. Fig. 20 shows the completed potential lead attachment and lead dressing. The same process is repeated on the other side of the strip while providing support under the strip with an aluminum plate suspended high enough to protect the connection on the other side.

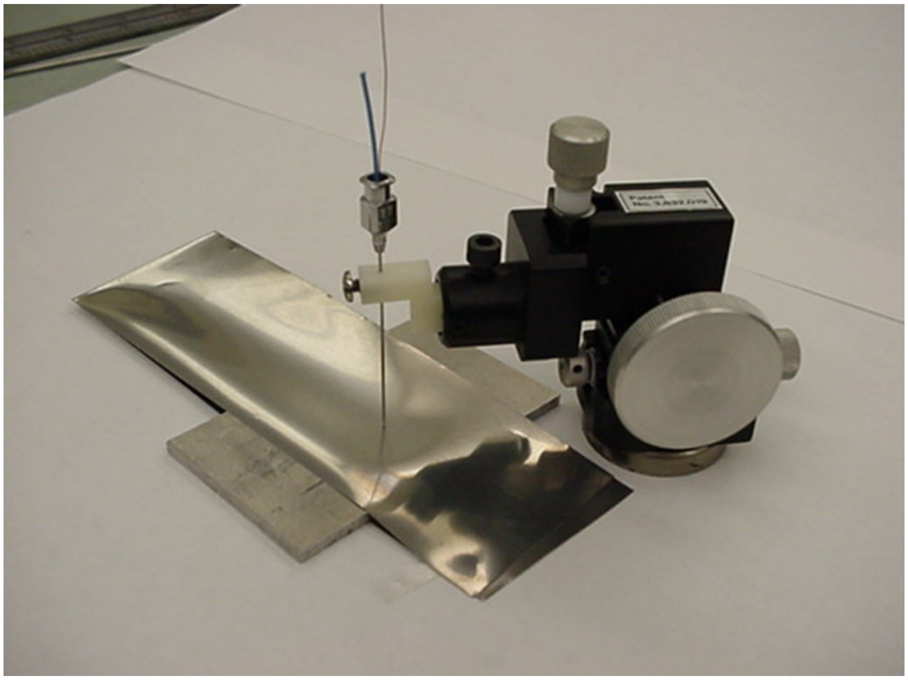

Figure 19. Photograph of set up used to hold and position potential wire prior to spot welding

Figure 20. Photograph of potential lead attached and dressed against resistance sheet

5.5 Attaching the current terminals

The last step in fabricating the resistance element is attaching copper end plates to each end of the strip. Refer to the Right and Left current plates in appendix A. Each copper plate is predrilled to accept a modified female/male type LC connector. Pre-tin the ends of the copper plates on the ends away from the holes using the same technique and dimensions described in tinning the resistance strip ends. Spread open the folded resistance strip and place the tinned end up on a hot plate. Place the tinned side of the copper plate down against the pre-tinned side of the resistance element overlapping only the tinned portion. Carefully align the copper plate with respect to the folded strip so that it is centered across the width and parallel to the long edge of the strip. Press the copper plate against the sheet and hot plate while checking again the alignment. Heat the joint and add a bit of extra solder until a smooth fillet is formed at the transition of the two metals. Align the second plate with pins through the predrilled holes with the first plate that has been soldered to one end of the strip. While maintaining the aligned position of the second plate on the strip, repeat the soldering process previously described. After soldering both current plates to the bifilar strip inspect the assembly to insure that the four mounting holes of each plate are in alignment.

5.6 Final Assembly

Select the pre-machined Left Side Heat Sink Block and lay the block on a surface with fins down. The two slots machined on the flat surface serve to provide a channel for the potential lead and a relief for the fold at the end of the strip. Cut two strips of elastomeric thermally conductive insulation material, Sil-Pad 2000, with a width slightly greater than the resistance strip and a length of 10.7 cm. Lay the insulation on the surface of the heat sink with one end flush with the inside edge of the slot near the end. The other end should be flush with the cutout relief end provided for the copper plates. Mark the position of the slot for the potential wire and cut a slot in the rubber equal to the width of the slot to about the center of the width. The slot in the rubber is intended to provide a relief for the potential connection and wire as can be seen in Fig. 20. Lay the Left Current Plate Backup insulator in the recess provided for the current terminals in the Left Side Heat Sink Block so that the holes align with the holes in the block. Lay the previously assembled bifilar strip with attached potential wires and current plates on top of the elastomer rubber with the Left Current Plate against the Left Side Backup insulator. Slide the Current Plate Separator Insulator between the Left and Right current plates.

Cut a strip of 0.025 mm (0.001”) Mylar insulator approximately 2 mm wider than the resistance strip and a length extending up to the first set of mounting holes in the current plates. Slip the dielectric insulator between the folded sheet and pull the end up as far as possible against the inside of the fold. Align the insulator so that an equal amount extends beyond both edges of the strip.

Lift up the Right current plate and insert four insulator bushings in the four holes of the Left current plate. Place at least two ¼-20 screws through the holes in the current plates and lightly tighten them against the Left Side Heat Sink Block with nuts. This insures that the resistance assembly becomes anchored and aligned in the Heat Sink Block. Check that the fold protrudes over the fold relief slot and that the potential wire against the element lies with the potential wire relief slot.

Before attaching the Right Side Heat Sink Block the potential wires should be attached to the potential connector. Screw into the Potential Connector Housing a type BNC connector with an insulated outer shell. Attach with one screw the Housing Block to the Left Side Heat Sink Block in the threaded hole provided on the edge. Cut, strip and solder the potential wires to the terminals on the BNC connector. Make sure that the potential wire attached on the left side (i.e. the potential connection closest to the Left Current Plate) is connected to the center pin of the BNC connector. This will insure that the polarity of the potential terminal is aligned with the polarity of the current terminal.

Lay the second precut elastomer rubber over the element aligned with the previously placed rubber that was placed on the Left Side Heat Sink Block. Position the Right Side Heat Sink Block over the assembly and align the ten clamping screw holes around the two edges of the heat sink blocks. Insert the clamping screws through the holes and four fan mounting brackets. Tighten the ten clamping screws with nuts using a torque wrench. Beginning with the middle screws, establish a build-up torqueing sequence from the center to outside screws ending with a final torque of 25 in-lbs.

Attach the modified female LC connector (see appendix A) to the current plates using appropriate length ¼-20 screws. The male LC connector is modified with a male center pin extension soldered to the male center pin. Screw the back shell of the modified male LC connector onto the female LC connector. Insert a ¼-20 nut through the hole provided in the Left Side Heat Sink Block and tighten onto the threaded end of the center pin extension. This completes the assembly process for the 0.1 Ω current shunt.

5.7 Troubleshooting Assembly Problems

After the unit has been assembled the shunt should be checked for functionality with a four-terminal resistance meter having a minimum resolution of 100 μΩ/Ω and automatic reversal capability to null out thermoelectric offsets. The shunt should indicate a resistance of 0.1 Ω ± 500 μΩ/Ω. Experience in constructing four shunts has shown that a 500 μΩ/Ω uncertainty in resistance from the intended value is about the best that can be achieved without resorting to trimming techniques. This is consistent with the uncertainties associated with the practicalities of locating the potential lead target points, lead placement, and welding.

Make sure that the polarity of resistance is consistent with the convention of positive current into the center pin of the LC connector producing a positive voltage at the center of the BNC potential terminal. If this is not the case it will be necessary to reverse the potential lead connections.

If the resistance measurement indicates a very high value it is likely that there is an open circuit somewhere in the potential circuit. Check for continuity at the BNC potential terminal and continuity through the weld joints. If the resistance measurement indicates a very low value of resistance it is likely that a short circuit has developed during the assembly process. If this is the case there is no alternative but to disassemble the shunt. A clue of where the problem might be is to monitor the resistance while loosening the clamping screws. If the resistance returns to normal either during loosening or removing the Right Side Heat Sink it is usually an indication that a short has developed across the dielectric material separating the sheets. It is advisable at this point to make sure that the potential wires are not shorted together at some point and that the resistance element is not making contact with the heat sink plates other than at the "low" side of the current terminal.

Experience has shown that shorts are most likely caused by foreign particles puncturing the thin dielectric material. Since it is practically impossible to locate the failure it is easiest to replace the existing dielectric material with a new sheet. Also, it is advisable to check the edges of the resistance sheet for possible sharp or ragged edges. The edges can be smoothed by using a fine abrasive. Before replacing the dielectric, swab the insides of the sheets with alcohol to rid any foreign material. Monitor the resistance after a new dielectric has been installed and continue to monitor the resistance while torquing the heat sink clamping screws.

6 MEASUREMENTS

6.1 Common measurement problems

The diagram shown in Fig 3, offers a generalized scheme of how differential measurements were made between the current shunt in question and a reference standard current transformer. It does not convey all of the nuances that may affect the absolute accuracy of a comparison measurement. The diagram assumes that the current circulating in the measurement loop is not detoured through ground loops or other unintended paths, and that the loading caused by the input impedance of the waveform measuring instrumentation is negligible. We know from practical experience that this is not always the case and may require extraordinary means to approach the best possible configuration.

In order to appreciate the possible pitfalls of comparing the performance of say, two 4-terminal current shunts against each other, consider the schematic in Fig. 21. This configuration represents possibly the worst condition where the measuring instrumentation must deal with differing and substantial common-mode voltages. Here the non-idealities of two identical measuring instruments are represented by input impedance Z_{in} and a low-terminal impedance to ground, $Z_{low.}$ Also, included are finite potential lead resistances, R_s. Because of the common mode voltage across $Z_{low,}$ a fraction the main current is diverted through a ground path. The result is that the current through the two shunts is not the same. Thus, the potential across shunt 2 will be in error by the amount of diverted current. Furthermore, an error is produced by any current in the potential terminals creating additional voltage drops that differ in the two shunts by the different common-mode voltages of each shunt.

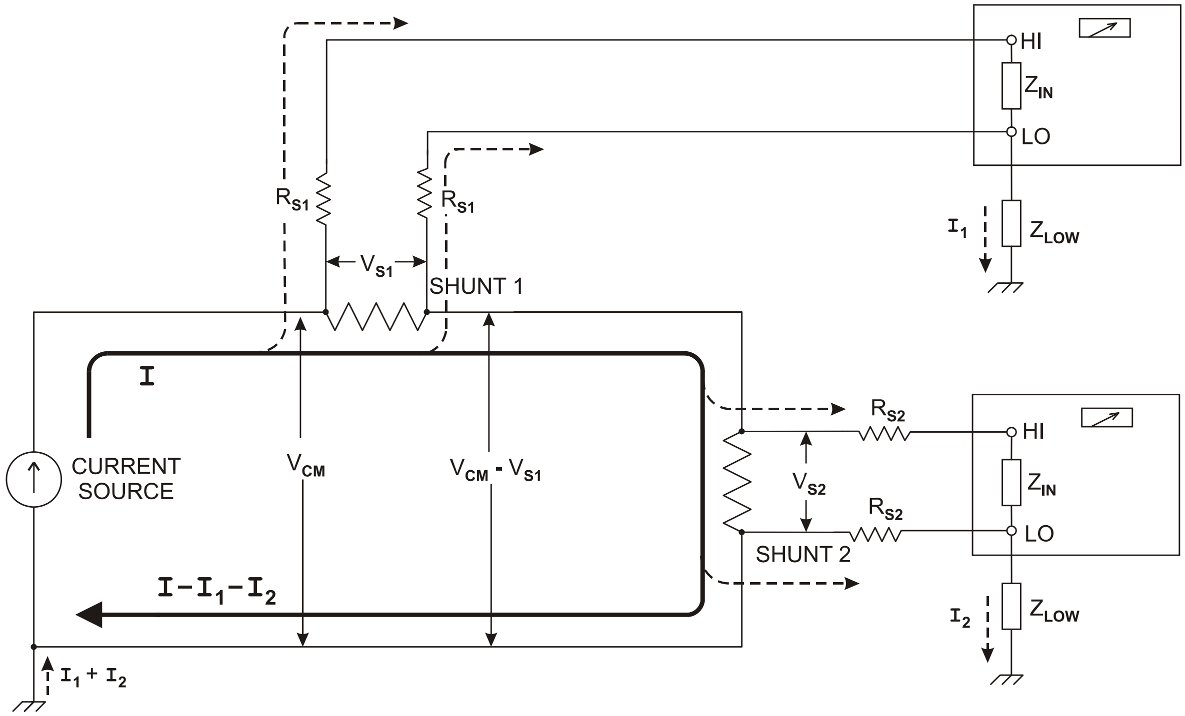

Figure 21. Diagram of voltages and loop currents involved in comparing two four-terminal shunts

If the measuring instruments are of a high quality differential input type so that the impedances Z_{in} and Z_{low} are essentially infinite, there is still one more error source to contend with and that is the common-mode rejection properties of the differential amplifiers. Common-mode rejection ratio (CMRR) is a measure of the capability of the measuring instrument to reject the common-mode signal. CMRR is important because it indicates the fraction of the common mode signal that is indicated or translated as a normal-mode signal. While the standard test methods for CMRR of differential amplifiers often specify a 1 kΩ resistance in the LO input, for this application it is more meaningful to connect one potential terminal to both differential inputs in the presence of the actual common mode voltage and observe the reading. CMRR of a differential amplifier is sensitive to frequency and tends to deteriorate with increased frequency. CMRR should be checked at all frequencies of interest.

Refer again to Fig. 3 where a four-terminal shunt is being compared against a CT. Note with respect to the common mode issues just described the advantage of placing the CT in the "high side" of the current loop. The voltage developed as a result of the drop across the shunt is the common mode voltage of the CT. Because of the inherent isolation properties of a CT the common mode voltage presented to the measuring instrument is greatly reduced and thus reducing the requirement for instruments with very high CMMR. Furthermore, leakage currents through the instrumentation to ground tend to be lower. However, at high frequencies even a small primary to secondary capacitance can allow significant leakage currents to ground. A test to insure that there are no sneak-paths of current is to monitor the outgoing and return currents of the source. A convenient way to do this is to place the outgoing and return current conductors from the source through the window of a wide band current transformer. If all of the outgoing current equals the return current then the secondary current should be zero. Any measured amount in the secondary is an indication that there are leakage current paths around the intend paths.

Thermal converters can be used to monitor the potential terminals of a shunt under test. They have the advantage of having excellent isolation properties in addition to well known characterized ac-dc differences. Their isolation properties are limited only by the small capacitance between the heater element and thermocouple. However, thermal converters are limited to measuring the ac-dc differences and are unable to provide any phase angle information. Shunts can be characterized either by direct comparison against a current thermal converter or a shunt thermal converter combination. Future work is anticipated which will be designed to compare the ac-dc difference of the calculable shunt against various thermal converter standards.

6.2 Power coefficient of resistance

The Evanohm resistance material selected for this application has a positive temperature coefficient of resistance of about 25 μΩ/Ω/^{o}C. This will affect the absolute accuracy of the shunt in two ways: changes in resistance due to ambient temperature changes and changes due to self heating effects. The latter is usually referred to as the power coefficient of resistance and is affected by the thermal resistance between the resistance element and the ambient. Fig. 22 shows the result of resistance changes that take place when the shunt is operated at 1 A and 10 A. The vertical axis indicates the deviation from 0.1 Ω in μΩ/Ω. The temperature of the heat sink was monitored throughout the test indicating about a 1.5 ^{0}C rise and a change in resistance of 58 μΩ/Ω. A time constant of about 10 minutes is indicated with over 30 minutes required to reach an equilibrium value of resistance.

For some metrology applications where the absolute value of resistance must be known to within a few μΩ/Ω over normal laboratory ambient temperature changes and different currents, it is possible to improve the performance by several different methods. The first is to choose or modify by annealing the resistance material for a lower temperature coefficient of resistance. Recent work has shown that greater resistance accuracy can be achieved by a thermal error correction model using the temperature of the heat sink as the variable that predicts the change in resistance. A more recent work has shown that thermal errors due both to ambient and power dissipation can be significantly reduced by using thermal-electric heater/coolers attached to the heat sinks in a control system that maintains the heat sink at a constant set-point temperature.

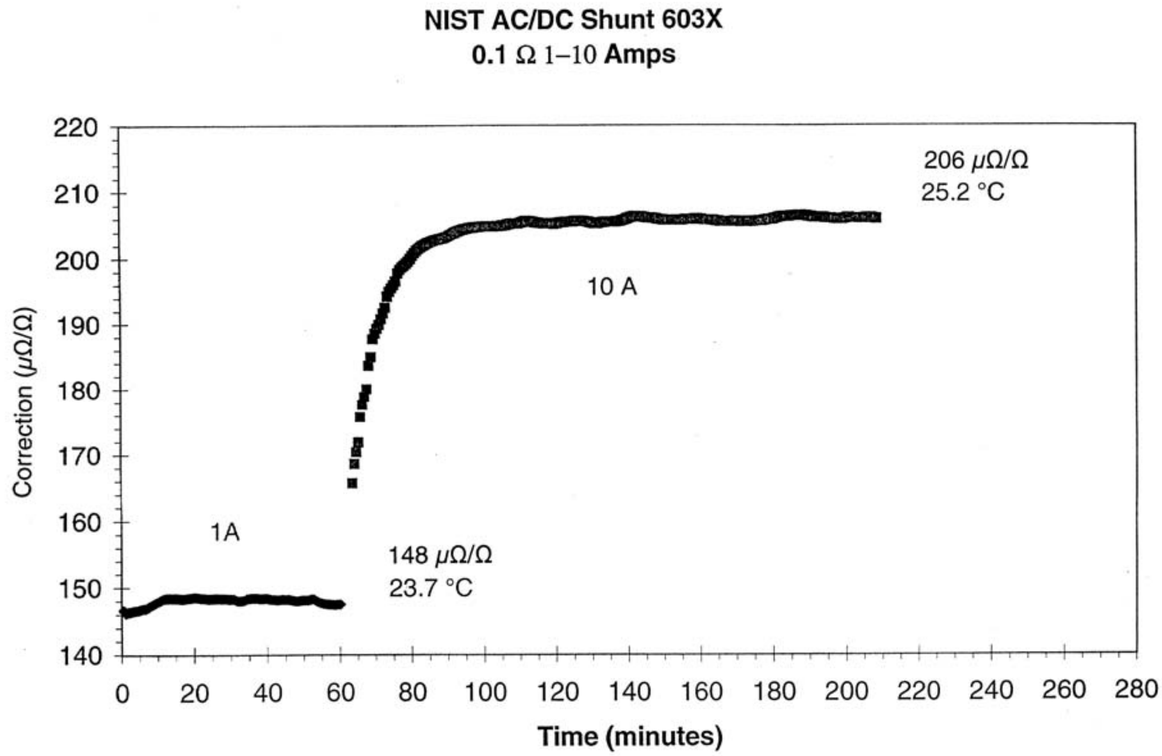

Figure 22. Plot of current shunt dc resistance change at 1 A and 10 A versus time

7. ACKNOWLEDGEMENT

The authors gratefully acknowledge the efforts of Nicholas Paulter who performed the finite element field modeling.

8. REFERENCES

[1] F. B. Silsbee, *A Study of the Inductance of Four-Terminal Resistance Standards*, NBS Scientific Paper No. 281, July 1916.

[2] F. B. Silsbee, *Notes on the Design of Four-Terminal Resistance Standards for Alternating Current*, NBS Journal of Research Paper No. 133, Vol. 4, January 1930.

[3] Ansoft, Maxwell® version 10

[4] F. J. Wilkins and M. L. Swan, "Precision AC/DC Resistance Standards," Proc. IEEE, Vol. 117, No. 4, April 1970, pp. 841-849.

APPENDIX A

Detailed Mechanical Drawings

A complete set of mechanical drawings suitable for replication of the Current Shunt described in this note are provided in this appendix.

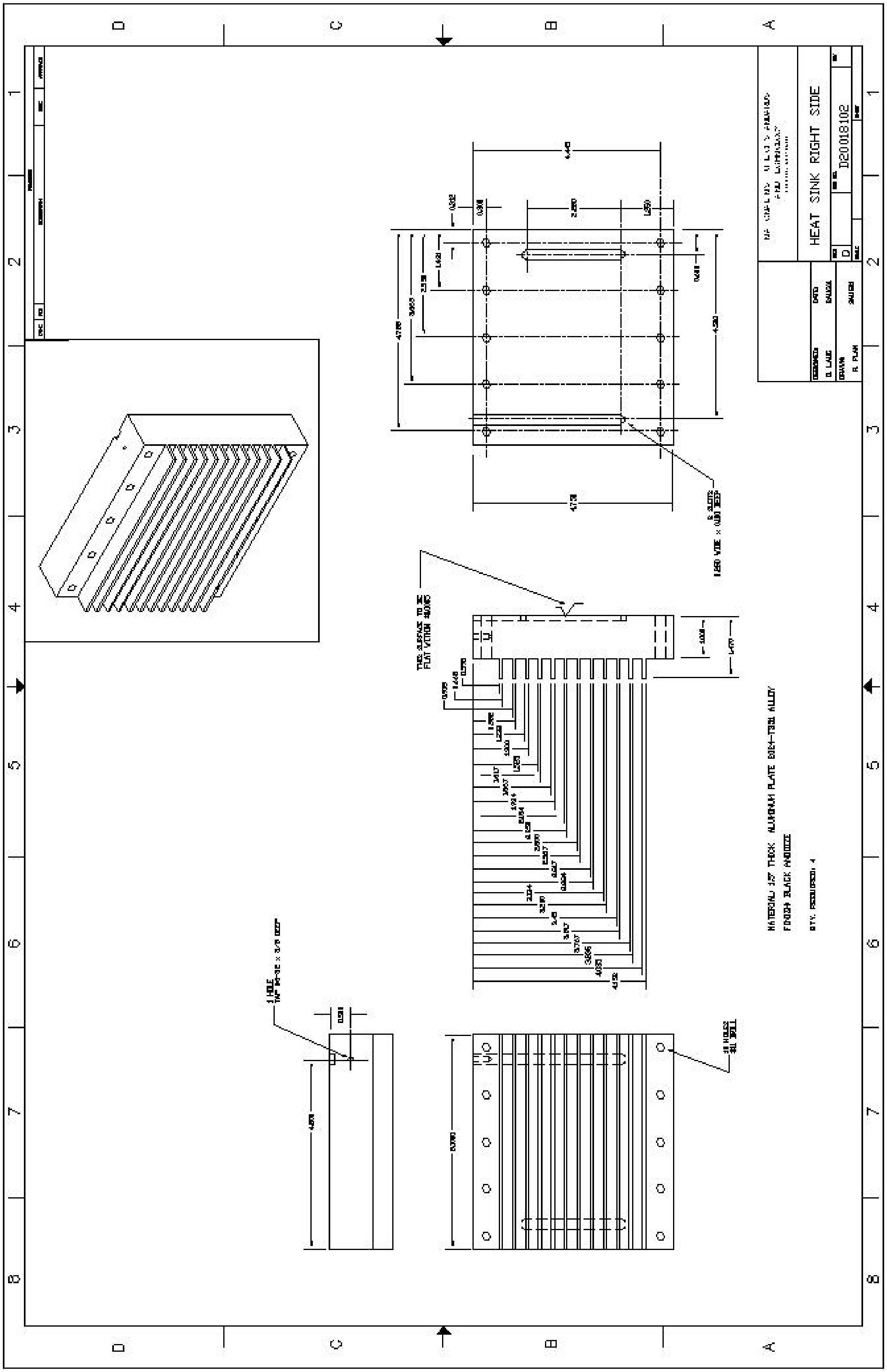
HEAT SINK RIGHT SIDE
D20018102

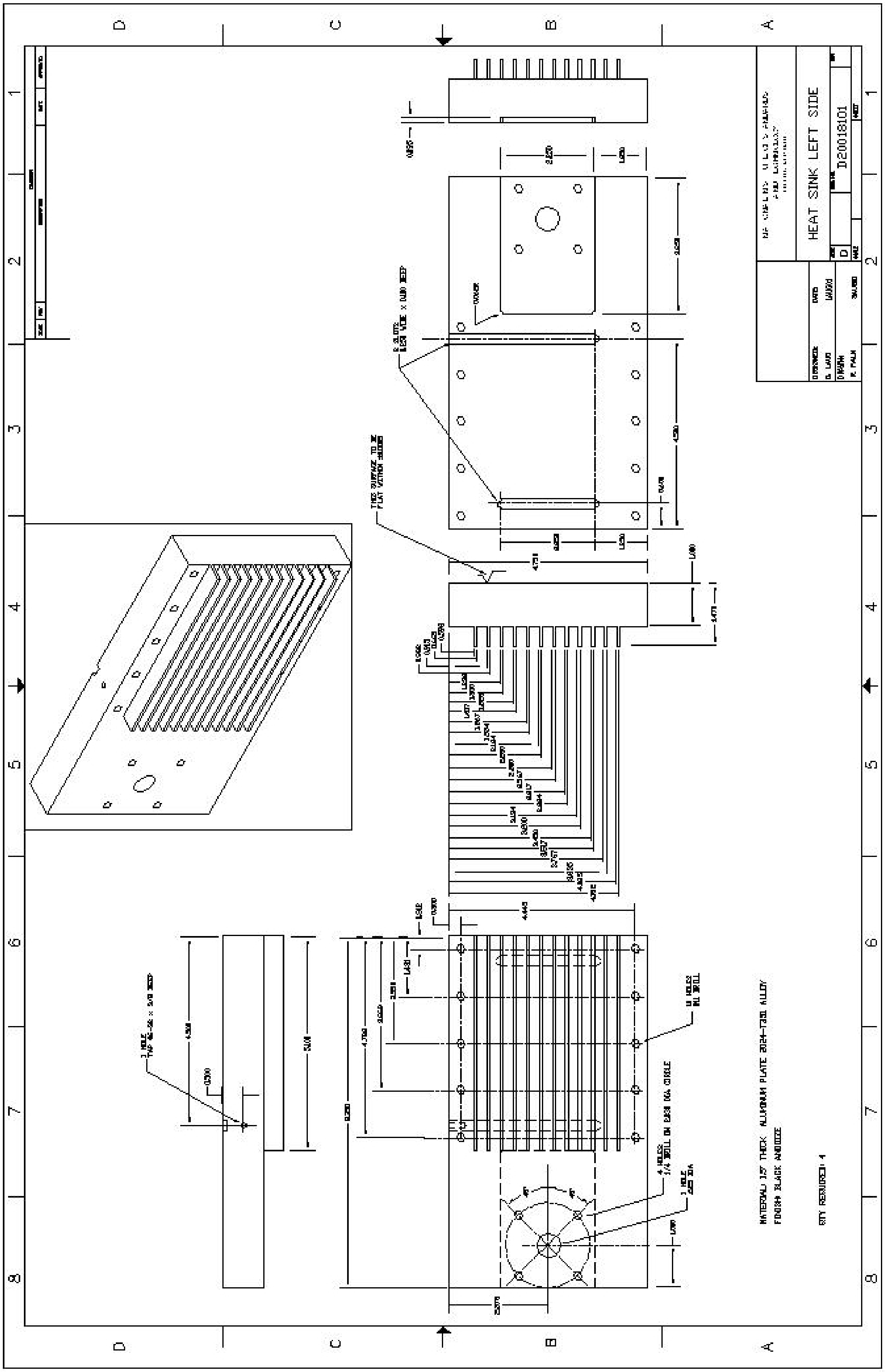
HEAT SINK LEFT SIDE
D20018101

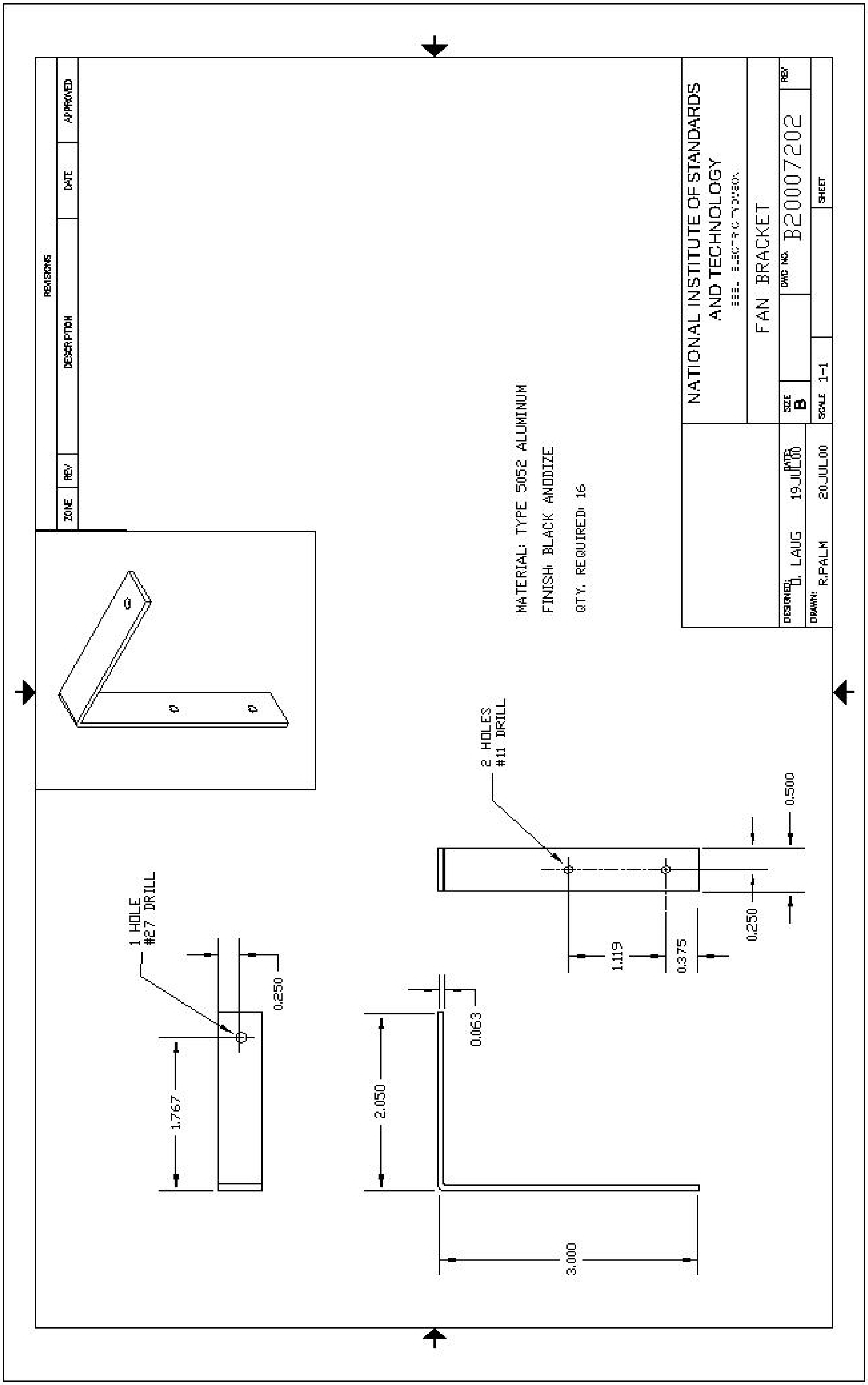
REVISIONS
ZONE
REV
DESCRIPTION
DATE
APPROVED
MATERIAL: TYPE 5052 ALUMINUM
FINISH: BLACK ANODIZE
QTY. REQUIRED: 16
2 HOLES
#11 DRILL
1 HOLE
#27 DRILL
0.500
0.250
1.119
0.375
0.250
0.063
1.767
2.050
3.000
NATIONAL INSTITUTE OF STANDARDS
AND TECHNOLOGY
FAN BRACKET
DESIGNED D. LAUG
DATE 19JUL00
DRAWN R.PALM
20JUL00
SIZE B
SCALE 1-1
DWG NO. B20007202
SHEET
REV

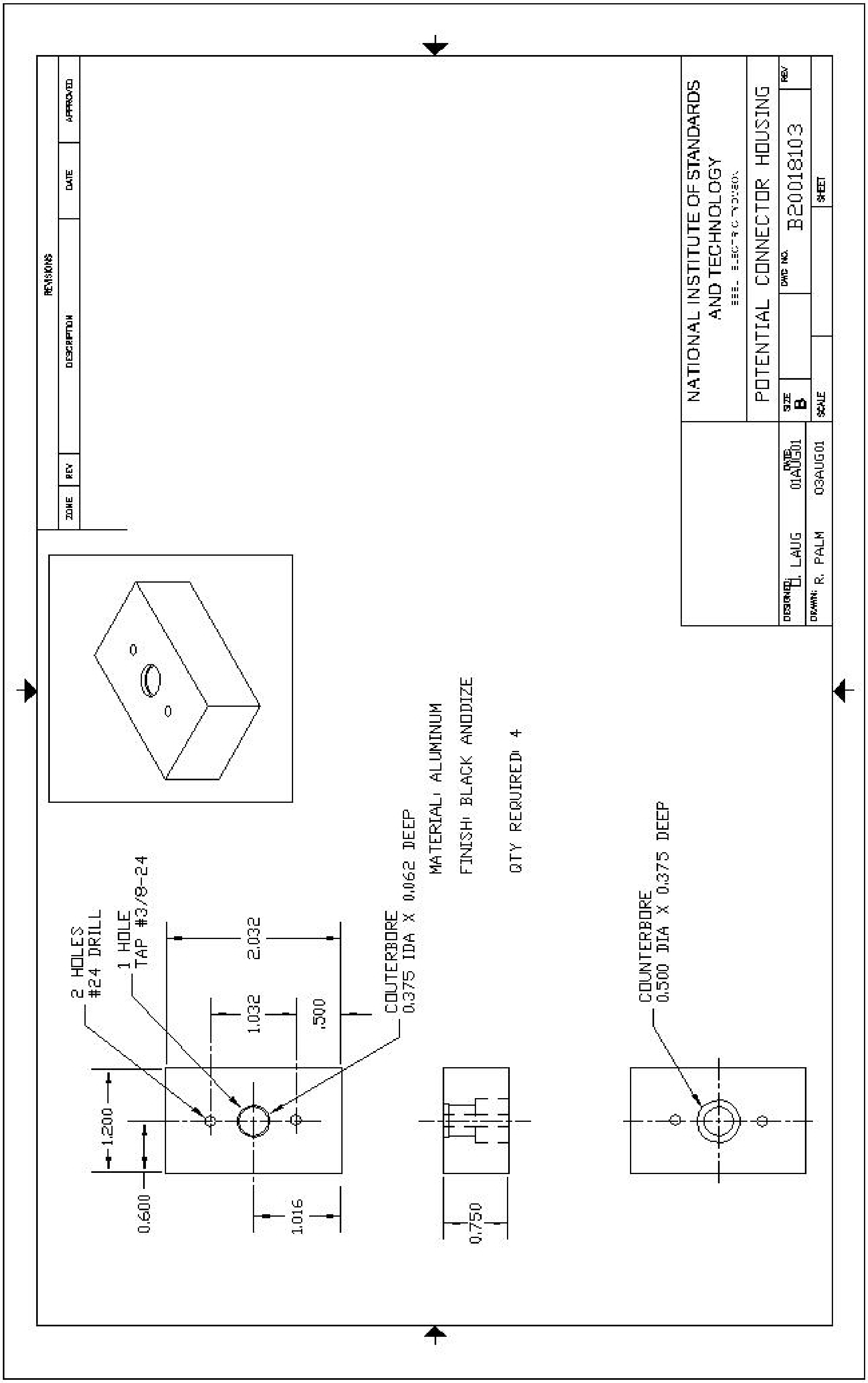
2 HOLES
#24 DRILL
1 HOLE
TAP #3/8-24
2.032
1.032
.500
COUTERBORE
0.375 IDA X 0.062 DEEP
MATERIAL: ALUMINUM
FINISH: BLACK ANODIZE
QTY REQUIRED: 4
1.200
0.600
1.016
0.750
COUNTERBORE
0.500 DIA X 0.375 DEEP
REVISIONS
ZONE
REV
DESCRIPTION
DATE
APPROVED
NATIONAL INSTITUTE OF STANDARDS
AND TECHNOLOGY
POTENTIAL CONNECTOR HOUSING
DESIGNED: D. LAUG
DATE: 01AUG01
DRAWN: R. PALM
03AUG01
SIZE B
DWG NO.
B20018103
REV
SCALE
SHEET

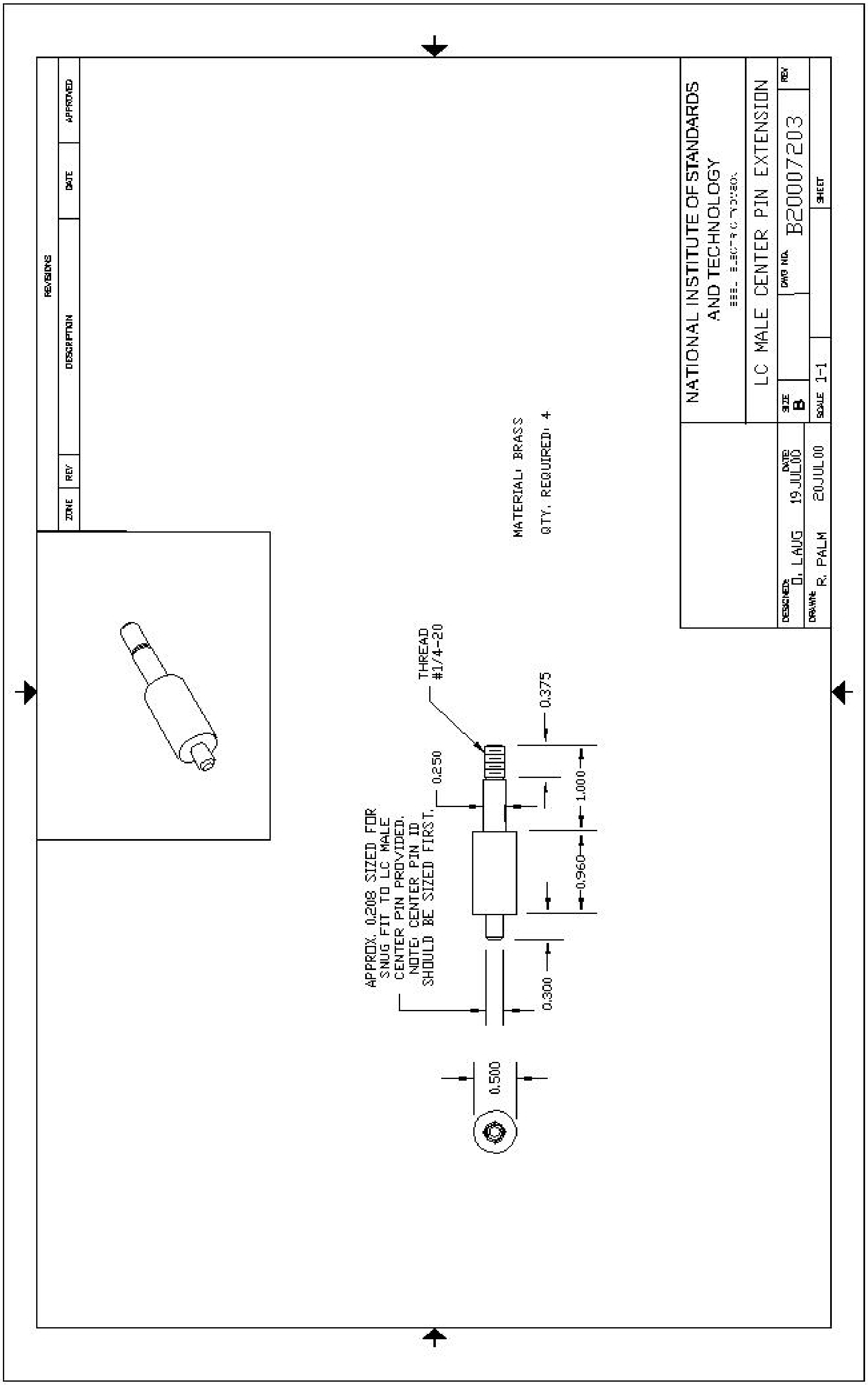

REVISIONS
ZONE
REV
DESCRIPTION
DATE
APPROVED
THREAD #1/4-20
0.375
0.250
1.000
0.960
0.300
0.500
APPROX. 0.208 SIZED FOR SNUG FIT TO LC MALE CENTER PIN PROVIDED. NOTE: CENTER PIN ID SHOULD BE SIZED FIRST.
MATERIAL: BRASS
QTY. REQUIRED: 4
NATIONAL INSTITUTE OF STANDARDS AND TECHNOLOGY
LC MALE CENTER PIN EXTENSION
SIZE B
DWG NO. B20007203
REV
SCALE 1-1
SHEET
DESIGNED D. LAUG
DATE 19JUL00
DRAWN R. PALM
20JUL00

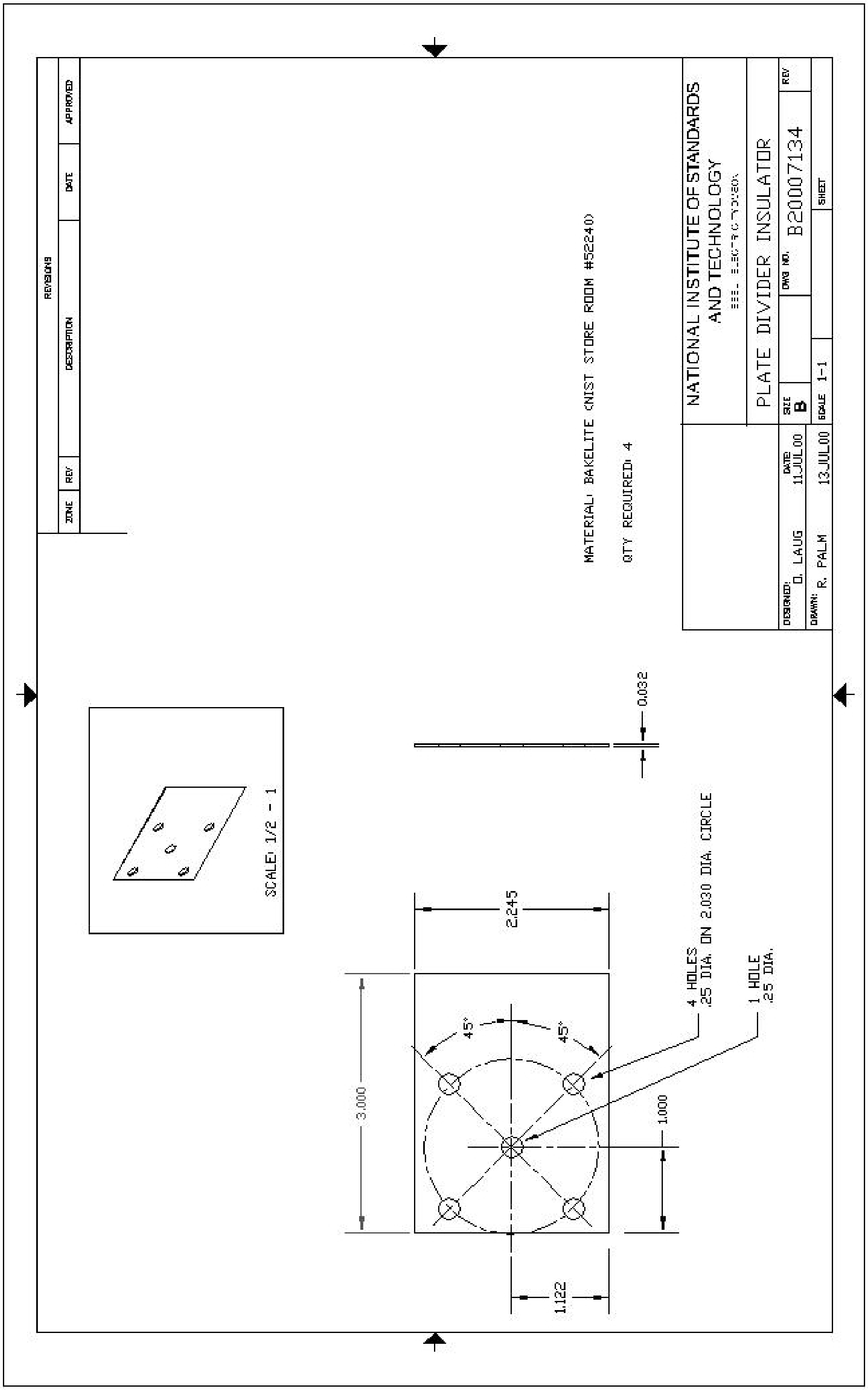
REVISIONS
ZONE
REV
DESCRIPTION
DATE
APPROVED
MATERIAL: BAKELITE (NIST STORE ROOM #52240)
QTY REQUIRED: 4
NATIONAL INSTITUTE OF STANDARDS
AND TECHNOLOGY
PLATE DIVIDER INSULATOR
SIZE B
DWG NO. B20007134
REV
DESIGNED: D. LAUG
DATE 11JUL00
DRAWN: R. PALM
13JUL00
SCALE 1-1
SHEET
0.032
SCALE: 1/2 - 1
2.245
3.000
45°
45°
4 HOLES
.25 DIA. ON 2.030 DIA. CIRCLE
1 HOLE
.25 DIA.
1.000
1.122

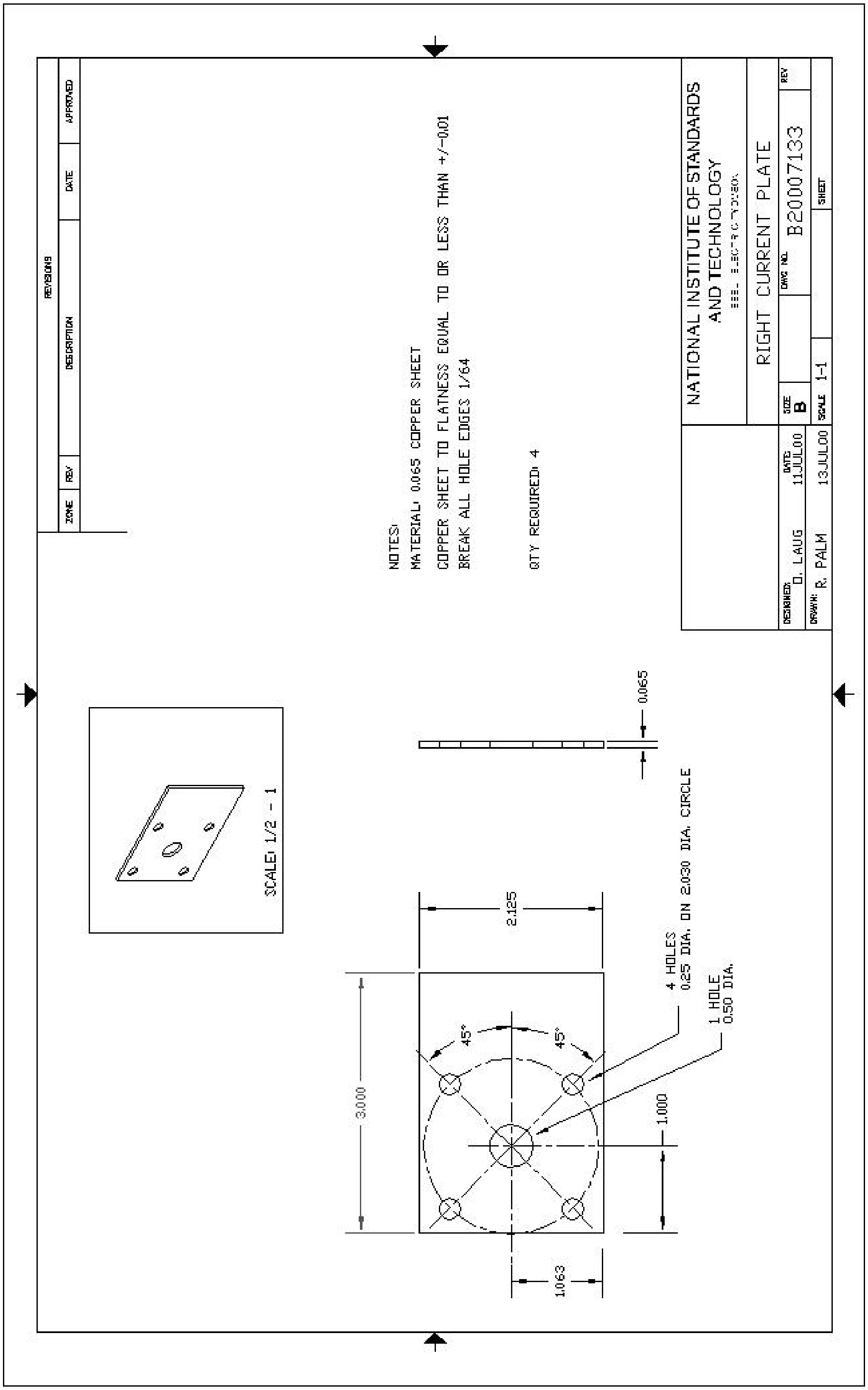
REVISIONS
ZONE
REV
DESCRIPTION
DATE
APPROVED
NOTES:
MATERIAL: 0.065 COPPER SHEET
COPPER SHEET TO FLATNESS EQUAL TO OR LESS THAN +/-0.01
BREAK ALL HOLE EDGES 1/64
QTY REQUIRED: 4
SCALE: 1/2 - 1
0.065
2.125
3.000
1.000
1.063
45°
45°
4 HOLES
0.25 DIA. ON 2.030 DIA. CIRCLE
1 HOLE
0.50 DIA.
NATIONAL INSTITUTE OF STANDARDS
AND TECHNOLOGY
RIGHT CURRENT PLATE
DESIGNED: D. LAUG
DATE: 11JUL00
DRAWN: R. PALM
13JUL00
SIZE B
DWG NO. B20007133
REV
SCALE 1-1
SHEET

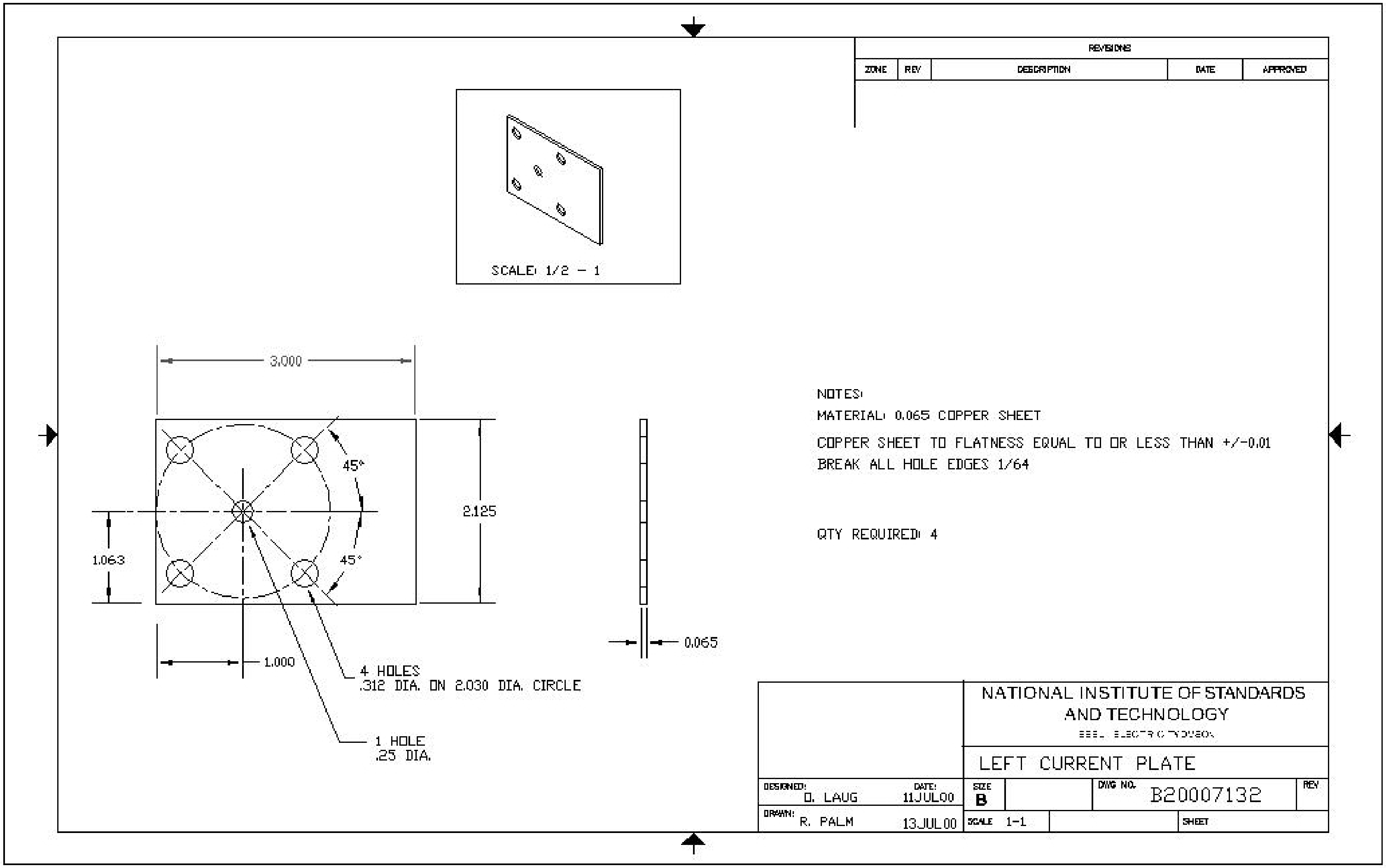
REVISIONS
ZONE
REV
DESCRIPTION
DATE
APPROVED
SCALE: 1/2 - 1
3.000
2.125
1.063
1.000
45°
45°
4 HOLES
.312 DIA. ON 2.030 DIA. CIRCLE
1 HOLE
.25 DIA.
0.065
NOTES:
MATERIAL: 0.065 COPPER SHEET
COPPER SHEET TO FLATNESS EQUAL TO OR LESS THAN +/-0.01
BREAK ALL HOLE EDGES 1/64
QTY REQUIRED: 4
NATIONAL INSTITUTE OF STANDARDS
AND TECHNOLOGY
LEFT CURRENT PLATE
DESIGNED: D. LAUG
DATE: 11JUL00
DRAWN: R. PALM
13JUL00
SIZE B
DWG NO. B20007132
REV
SCALE 1-1
SHEET

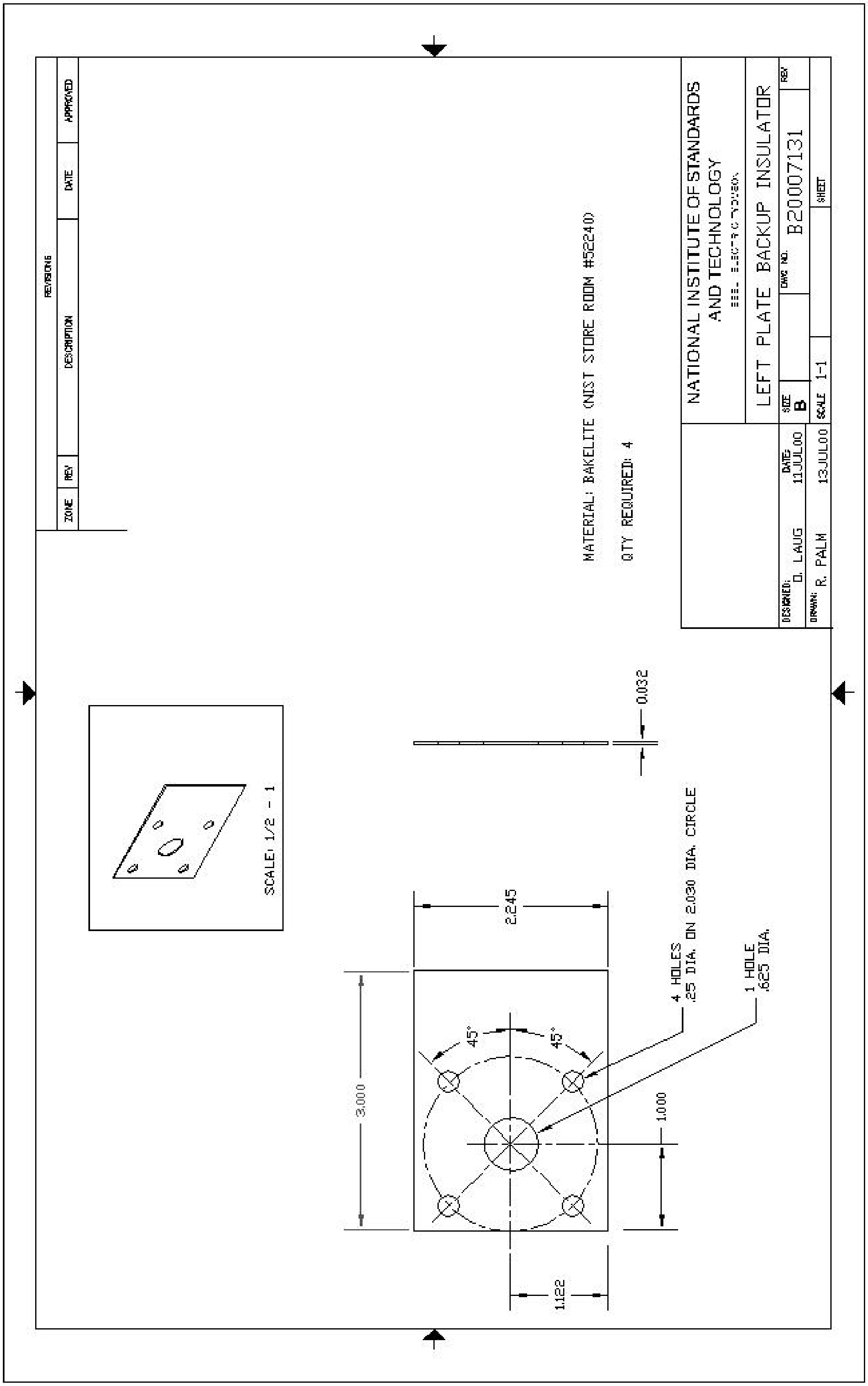

REVISIONS
ZONE
REV
DESCRIPTION
DATE
APPROVED
MATERIAL: BAKELITE (NIST STORE ROOM #52240)
QTY REQUIRED: 4
SCALE: 1/2 - 1
0.032
2.245
3.000
1.000
1.122
45°
45°
4 HOLES
.25 DIA. ON 2.030 DIA. CIRCLE
1 HOLE
.625 DIA.
NATIONAL INSTITUTE OF STANDARDS
AND TECHNOLOGY
LEFT PLATE BACKUP INSULATOR
DESIGNED: D. LAUG
DATE: 11JUL00
DRAWN: R. PALM
13JUL00
SIZE B
DWG NO. B20007131
REV
SCALE 1-1
SHEET

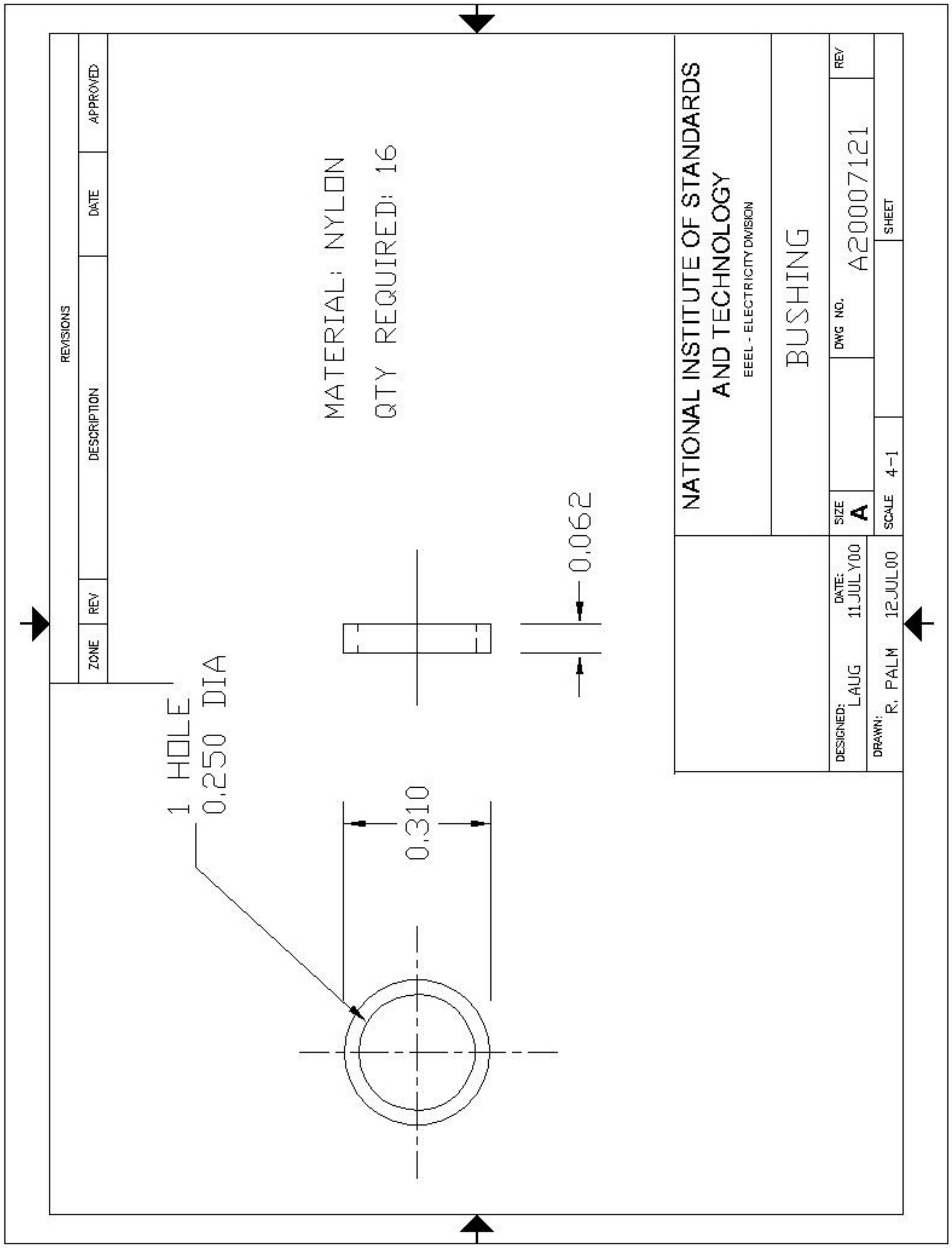
REVISIONS
ZONE
REV
DESCRIPTION
DATE
APPROVED
MATERIAL: NYLON
QTY REQUIRED: 16
1 HOLE
0.250 DIA
0.310
0.062
NATIONAL INSTITUTE OF STANDARDS
AND TECHNOLOGY
EEEL - ELECTRICITY DIVISION
BUSHING
DESIGNED:
LAUG
DATE:
11JULY00
DRAWN:
R. PALM
12JUL00
SIZE
A
DWG NO.
A20007121
REV
SCALE 4-1
SHEET

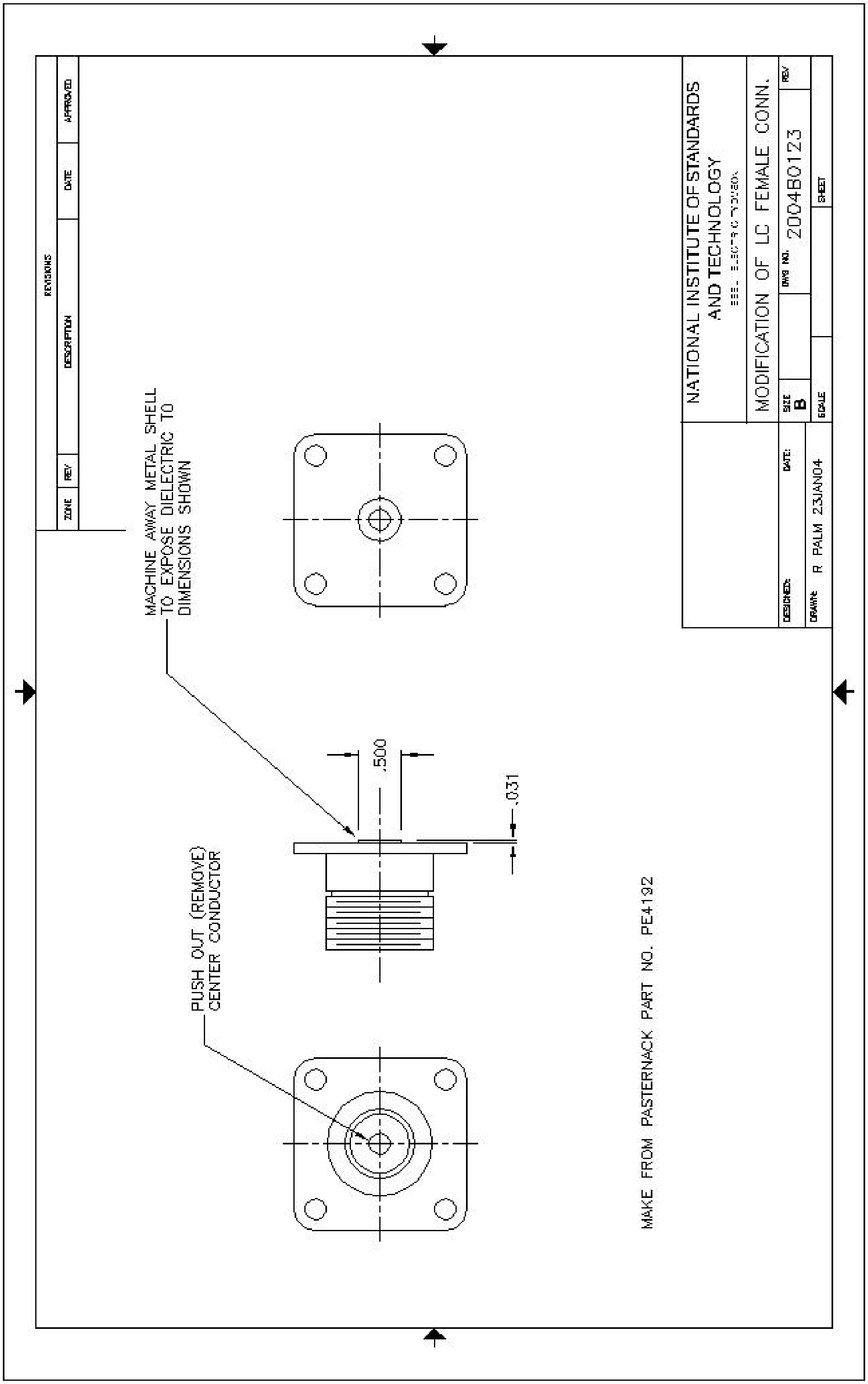
REVISIONS
ZONE
REV
DESCRIPTION
DATE
APPROVED
MACHINE AWAY METAL SHELL TO EXPOSE DIELECTRIC TO DIMENSIONS SHOWN
.500
.031
PUSH OUT (REMOVE) CENTER CONDUCTOR
MAKE FROM PASTERNACK PART NO. PE4192
NATIONAL INSTITUTE OF STANDARDS AND TECHNOLOGY
MODIFICATION OF LC FEMALE CONN.
DESIGNED:
DATE:
DRAWN: R PALM 23JAN04
SIZE B
DWG NO. 2004B0123
REV
SCALE
SHEET